ลักษณะเฉพาะของพลาสมาและสมรรถนะการกัดด้วยไอออนในกระบวนการผลิต ฮาร์ดดิสก์ไดรฟ์สไลเดอร์

นายนภกานต์ วงศ์พาณิชย์

บทคัดย่อและแฟ้มข้อมูลฉบับเต็มของวิทยานิพนธ์ตั้งแต่ปีการศึกษา 2554 ที่ให้บริการในคลังปัญญาจุฬาฯ (CUIR)
เป็นแฟ้มข้อมูลของนิสิตเจ้าของวิทยานิพนธ์ ที่ส่งผ่านทางบัณฑิตวิทยาลัย
The abstract and full text of theses from the academic year 2011 in Chulalongkorn University Intellectual Repository (CUIR)
are the thesis authors' files submitted through the University Graduate School.

วิทยานิพนธ์นี้เป็นส่วนหนึ่งของการศึกษาตามหลักสูตรปริญญาวิทยาศาสตรมหาบัณฑิต
สาขาวิชาฟิสิกส์ ภาควิชาฟิสิกส์
คณะวิทยาศาสตร์ จุฬาลงกรณ์มหาวิทยาลัย
ปีการศึกษา 2560

ลิขสิทธิ์ของจุฬาลงกรณ์มหาวิทยาลัย

PLASMA CHARACTERISTICS AND ION ETCHING PERFORMANCE IN HARD DISK DRIVE SLIDER FABRICATION PROCESSES

จุฬาลงกรณ์มหาวิทยาลัย
Chulalongkorn University

Mr. Napakan Wongpanit

A Thesis Submitted in Partial Fulfillment of the Requirements

for the Degree of Master of Science Program in Physics

Department of Physics

Faculty of Science

Chulalongkorn University

Academic Year 2017

Copyright of Chulalongkorn University

Thesis Title	PLASMA CHARACTERISTICS AND ION ETCHING PERFORMANCE IN HARD DISK DRIVE SLIDER FABRICATION PROCESSES
By	Mr. Napakan Wongpanit
Field of Study	Physics
Thesis Advisor	Assistant Professor Sukkaneste Tungasmita, Ph.D.

Accepted by the Faculty of Science, Chulalongkorn University in Partial Fulfillment of the Requirements for the Master's Degree

.... Dean of the Faculty of Science

(Associate Professor Polkit Sangvanich, Ph.D.)

THESIS COMMITTEE

.... Chairman

(Varagorn Hengpunya, Ph.D.)

.... Thesis Advisor

(Assistant Professor Sukkaneste Tungasmita, Ph.D.)

.... Examiner

(Associate Professor Somchai Kiatgamolchai, Ph.D.)

.... External Examiner

(Pattira Homhuan, Ph.D.)

จุฬาลงกรณ์มหาวิทยาลัย
Chulalongkorn University

นภกานต์ วงศ์พาณิชย์ : ลักษณะเฉพาะของพลาสมาและสมรรถนะการกัดด้วยไอออนในกระบวนการผลิตฮาร์ดดิสก์ไดรฟ์สไลเดอร์ (PLASMA CHARACTERISTICS AND ION ETCHING PERFORMANCE IN HARD DISK DRIVE SLIDER FABRICATION PROCESSES) อ.ที่ปรึกษาวิทยานิพนธ์หลัก: ผศ. ดร. สุคคเณศ ตุงคะสมิต, 61 หน้า.

ฮาร์ดดิสก์ไดรฟ์เป็นหน่วยเก็บข้อมูลถาวรและเป็นส่วนประกอบสำคัญของคอมพิวเตอร์ อุปกรณ์อิเล็กทรอนิกส์ รวมไปถึงของแหล่งบริการเก็บข้อมูลแบบคลาวด์ การอ่านและเขียนข้อมูลทำงานได้โดยส่วนที่ใช้อ่าน และเขียนของฮาร์ดดิสก์ไดรฟ์สไลเดอร์ ส่วนที่ใช้อ่านและเขียนข้อมูลทำมาจากฟิล์มบางหลายๆชั้นของวัสดุที่แตกต่างกัน โดยเรียกรวมกันว่าอุปกรณ์ทันเนลลิ่งแมกนีโทรีซิสทีฟ ในกระบวนการผลิตฮาร์ดดิสก์ไดรฟ์สไลเดอร์ การเตรียมพื้นผิวและการทำความสะอาดในหลายๆขั้นตอนของการผลิตสามารถทำได้โดยการใช้กระบวนการกัดด้วยลำไอออน ในการศึกษานี้ได้มีการนำชุดโปรแกรมสถานการณ์จำลองที่อาศัยพื้นฐานการคำนวณแบบมอนติคาร์โลมาคำนวณค่ายีลด์ที่เกิดจากการกัดของไอออนและเปอร์เซ็นการสูญเสียพลังงานจากการกัดของวัสดุเหล่านั้นในโครงสร้างของทันเนลลิ่งแมกนีโทรีซิสทีฟ ซึ่งจากการจำลองพบว่าค่ายีลด์ของการกัดมีค่ามากที่สุดเมื่อใช้มุมตกกระทบของลำไอออนที่ 70 อาศาที่นับจากเส้นแนวฉากของพื้นผิววัสดุ ค่ายีลด์ของการกัดรวมของสารประกอบถูกคำนวณมาจากยีลด์ของแต่ละธาตุที่ได้จากการจำลอง การศึกษาสมบัติพลาสมาในระบบการกัดด้วยลำไอออนของระบบระดับอุตสาหกรรมจึงถูกนำมาศึกษาในเงื่อนไขต่างๆที่ใช้ในระบบการผลิต ผลกระทบจากตัวแปรในระบบอันได้แก่ มุมตกกระทบของลำไอออน กระแสของไอออน และอัตราการไหลของแก๊สอาร์กอนในระบบได้ถูกนำมาวิเคราะห์ ซึ่งผลการวิเคราะห์ลักษณะเฉพาะนี้พบว่า ค่าศักย์ไฟฟ้าลอย ของระบบที่มีการชดเชยปริมาณอิเล็กตรอนจากพลาสมาบริดจ์นิวทรัลไลเซอร์ มีค่าประมาณ 3 โวลต์ ขณะที่ค่าของศักย์พลาสมา มีค่า 2.5 โวลต์ ค่าความหนาแน่นกระแสของไอออนในระบบจริงและอัตราการถูกกัดของวัสดุทันเนลลิ่งแมกนีโทรีซิสทีฟที่แตกต่างกันได้ถูกคำนวณออกมา

ภาควิชา	ฟิสิกส์	ลายมือชื่อนิสิต	....
สาขาวิชา	ฟิสิกส์	ลายมือชื่อ อ.ที่ปรึกษาหลัก	....
ปีการศึกษา	2560		

／／ 5772021023 : MAJOR PHYSICS
KEYWORDS: PLASMA CHARACTERIZATION / ION BEAM ETCHING / MULTILAYER THIN FILM PROCESS

NAPAKAN WONGPANIT: PLASMA CHARACTERISTICS AND ION ETCHING PERFORMANCE IN HARD DISK DRIVE SLIDER FABRICATION PROCESSES. ADVISOR: ASST. PROF. SUKKANESTE TUNGASMITA, Ph.D., 61 pp.

A hard disk drive (HDD) is the permanent magnetic data storage and one of the most important components of computers, electronic devices and cloud data storage service facility. The data reading and writing are operated by the reader and writer parts of HDD head or slider. These reader and writer were made of multilayer thin ilms of different materials, forming a tunneling magnetoresistive (TMR) device. In HDD production, the ion beam etching (IBE) process was used in the preparation of surface patterns and cleaning in many fabrication steps. The Monte Carlo-based simulation package, SRIM was applied to calculate the etching yields and %energy loss of those materials in the TMR structure. The calculation showed that the etching yields of materials reach the maximum value, at an incident angle of 70° to the normal surface. The total etching yields of compounds were calculated from the etching yield of each element. The plasma characterization in an industrial-size IBE system has been performed to extract the plasma characteristic at different process conditions. The effects of process parameters in IBE system such as incident beam angle, ion beam current and gas flow in the system were analyzed. The floating potential of plasma in this IBE system with the electron compensation from a plasma bridge neutralizer (PBN) is 3 V, while the plasma potential is 2.5 V. The ion current densities in the actual system and the etching rate of different TMR materials were calculated.

Department:	Physics	Student's Signature	....
Field of Study:	Physics	Advisor's Signature	....
Academic Year:	2017		

จุฬาลงกรณ์มหาวิทยาลัย
CHULALONGKORN UNIVERSITY

ACKNOWLEDGEMENTS

I would like to express my deep gratitude to my advisor, Assistant Professor Dr. Sukkaneste Tungasmita for his patience, understanding, encouragement, kindness, friendly and useful suggestions discussion during this work.

I wishes to greatly thank Dr. Varagorn Hengpunya for being the chairman, Assoc.Prof.Dr. Somchai Kiatgamolchai and Dr. Pattira Homhuan for being committee members of this thesis.

I would like to specially thank Mr. Amnart Chantron for teaching and training me to use the industrial-size IBE system.

I would like to thank Western Digital (Thailand) Co., Ltd. for the device supports.

I would also take this opportunity to thanks the Department of Physics, Faculty of science, Chulalongkorn University for providing financial support and the grants to accomplish this thesis. The department sponsored me for expenses to attend the conferences.

I would like to thank the Science Achievement Scholarship of Thailand (SAST) for supporting my tuitions and research budgets in this work.

Finally, the author is thankful to my family and friends for their love, understanding, inspiration, guidance, encouragement and support throughout my entire study.

CONTENTS

Page

THAI ABSTRACT iv

ENGLISH ABSTRACT v

ACKNOWLEDGEMENTS vi

CONTENTS vii

LIST OF TABLES ix

LIST OF FIGURES x

CHAPTER I INTRODUCTION ix

1.1 Motivation ix

1.2 Purposes of thesis x

1.3 Scope of this thesis x

1.4 Process of this thesis xi

CHAPTER II THEORETICAL BACKGROUND 1

2.1 Introduction to Hard Disk Drive (HDD) 1

2.2 Basic of plasma 4

2.3 Principle of sputtering/ion etching 6

2.4 Ion Beam Etching (IBE) 9

2.5 Plasma characterization 14

2.6 Plasma characteristics 16

2.7 Concept of simulation 21

CHAPTER III SIMULATIONS AND EXPERIMENTS 23

3.1 Plasma etching simulation 23

3.2 Experimental details on plasma characterization 25

จุฬาลงกรณ์มหาวิทยาลัย
CHULALONGKORN UNIVERSITY

Page

CHAPTER IV RESULTS AND DISCUSSION 28

4.1 Etching yield simulations 28

4.2 Plasma characterizations in IBE system 36

4.3 Ion current density calculations 44

4.4 Etching rate calculations 46

CHAPTER V SUMMARY AND CONCLUSION 54

REFERENCES 56

APPENDICES 59

Appendix A Conference Presentation 60

VITA 61

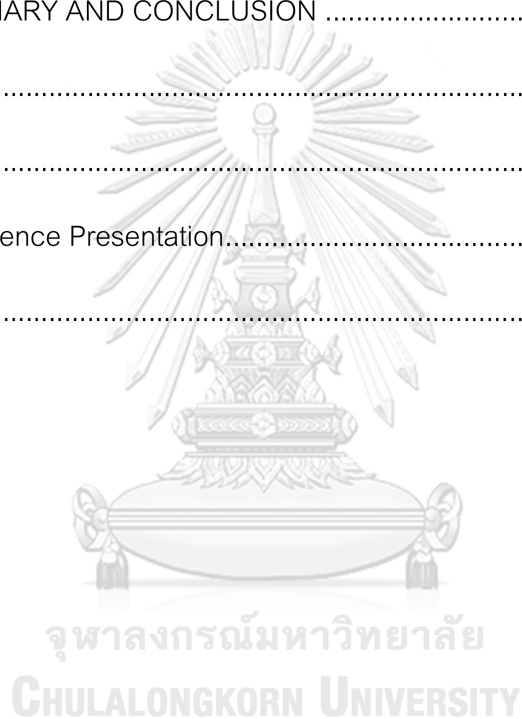

จุฬาลงกรณ์มหาวิทยาลัย
Chulalongkorn University

LIST OF TABLES

Page

Table 1 Plasma composition..4

Table 2 The conditions of input parameters. 23

Table 3 The obtained ion saturation current from experiments with the argon flow in an ion source and PBN are 20 sccm and 16 sccm, respectively. 45

Table 4 The calculated ion current densities (j_p) with the argon flow in an ion source and PBN are 20 sccm and 16 sccm, respectively. 46

LIST OF FIGURES

Page

Figure 1 A schematic of components of a hard disk drive (Canada, 2017). 1

Figure 2 (a) A HDD slider located above a platter, and (b) an ABS under the surface (Kubina, 2006)-(Damjanović). 2

Figure 3 (a) A Schematic of the multilayer stack composition in a HDD slider (J. R. Childress, 2006). (b) A multilayer of TMR device by TEM (Toyoo Miyajima, 2010). 3

Figure 4 An argon plasma in IBE system. 6

Figure 5 A schematic of sputtering process... 6

Figure 6 Directionality of etching. 10

Figure 7 (a) A schematic of the set of ion-optic grids and (b) their final energy of the accelerated ions. 12

Figure 8 An industrial-size IBE system with the ions/electrons compensation by a PBN. 14

Figure 9 Langmuir probe 14

Figure 10 The ideal I-V curve. 18

Figure 11 A plot of ln|I| versus a bias potential. 19

Figure 12 The paths of phosphorus ions that are hitting a silicon material (Ziegler et al., 2008). 21

Figure 13 The argon ions which penetrate near the surface of $Ni_{81}Fe_{19}$ target at the ion incident angle of (a) 75° and (b) 0° (normal to the surface of a target). 22

Figure 14 Simulation interface panel. 24

Figure 15 The percentage of energy loss during simulation. 25

จุฬาลงกรณ์มหาวิทยาลัย
Chulalongkorn University

Figure 16 (a) A schematic representation of the experimental setup. (b) A schematic representation of the special flat/wire plasma probe's circuit. 26

Figure 17 The definition of the incident beam directions though out from grids – (a) +20°, (b) 0° (normal to the surface) and (c) -30°. 27

Figure 18 Plots of the calculated etching yields and backscattered ions versus angle of the argon ions incident on $Co_{90}Fe_{10}$ material using SRIM. 30

Figure 19 Plots of the calculated etching yields and backscattered ions versus angle of the argon ions incident on $Co_{75}Fe_{25}$ material using SRIM. 30

Figure 20 Plots of the calculated etching yields and backscattered ions versus angle of the argon ions incident on $Ni_{81}Fe_{19}$ material using SRIM. 31

Figure 21 Plots of the calculated etching yields versus angle of the argon ions incident on MgO material using SRIM. 31

Figure 22 Plots of the calculated etching yields versus angle of the argon ions incident on $Ir_{21}Mn_{79}$ material using SRIM. 32

Figure 23 Plots of the calculated etching yields versus angle of the argon ions incident on $Ir_{24}Mn_{76}$ material using SRIM. 32

Figure 24 Plots of energy loss of incident ions. 33

Figure 25 Simulated etching yields of materials at +20°. 35

Figure 26 Simulated etching yields of materials at normal angle 0°. 35

Figure 27 Simulated etching yields of materials at -30°. 36

Figure 28 An I-V curve with a beam voltage, a beam current, an argon gas flow in PBN and an argon gas flow in a source are set as 400 volts, 800 mA, 6 sccm and 20 sccm respectively. 38

Figure 29 A floating potential and plasma potential observation. 38

จุฬาลงกรณ์มหาวิทยาลัย
Chulalongkorn University

Figure 30 Plasma I-V curves of combinations of beam voltage and current, simultaneously with an argon gas flow in PBN and an argon gas flow in a source are set 6 sccm and 20 sccm respectively. The ion impact angle was at normal incident angle for all cases. 39

Figure 31 Plasma I-V curves at different beam currents with a beam voltage, an argon gas flow in PBN and an argon gas flow in a source are set as 400 V, 6 sccm and 20 sccm respectively. The ion impact angle was at normal incident angle for all cases. 40

Figure 32 Plasma I-V curves at different beam voltages with a beam current, an argon gas flow in PBN and an argon gas flow in a source are set as 400 mA, 6 sccm and 20 sccm respectively. The ion impact angle was at normal incident angle for all cases. 41

Figure 33 An I-V curve with a beam current, beam vlotage and an argon gas flow in a source are set as 600 mA, 600 V and 20 sccm respectively at normal incident angle. 42

Figure 34 (a) An I-V curve with a beam current, beam voltage were set as 600 mA, 600 V and an argon gas flow in a source were 6 sccm respectively at normal incident angle. (b) Plots between I_{is} and argon flow in an ion source. 43

Figure 35 The (a) circular-flat probe and (b) wire probe used in measurements. 45

Figure 36 Etching rates of materials which are ordered by the conditions in the actual process. These rates are calculated by using the incident angle of +20º. 47

Figure 37 Etching rates of materials which are ordered by the conditions in the actual process. These rates are calculated by using the incident angle of 0º. 47

Figure 38 Etching rates of materials which are ordered by the conditions in the actual process. These rates are calculated by using the incident angle of -30º. 48

Figure 39 Etching rate of $Co_{90}Fe_{10}$ material. 50

Figure 40 Etching rate of $Co_{75}Fe_{25}$ material. 50

Figure 41 Etching rate of $Ni_{81}Fe_{19}$ material. 51

Figure 42 Etching rate of MgO material. 51

Figure 43 Etching rate of $Ir_{21}Mn_{79}$ material. 52

Figure 44 Etching rate of $Ir_{24}Fe_{76}$ material. 52

จุฬาลงกรณ์มหาวิทยาลัย
Chulalongkorn University

CHAPTER I

INTRODUCTION

1.1 Motivation

A hard disk drive (HDD) is the permanent magnetic data storage and one of the most important components in computers, electronic devices and cloud data storage service facilities. Inside the HDD, there are many parts that work together. One of the crucial parts in HDD is the head, containing data reader and writer so called "slider". The reader and writer are made of a multilayer thin film of different materials on the Al_2O_3-TiC (AlTiC) substrate. For modern read/write head, it uses the tunneling magnetoresistive (TMR) technology, which changes the resistance of a material in the presence of magnetic field [1-3]. Since the HDD slider fabrication influences a quality and reliability of HDDs, it is very important to develop the fabrication processes as well. An ion beam etching (IBE) process is commonly chosen to fabricate a slider's pattern underneath the slider in form of an air bearing surface (ABS) making the slider floats or slides at a few nanometers over the surface of a HDD's platter [4-6].

จุฬาลงกรณ์มหาวิทยาลัย
Chulalongkorn University

At the HDD reader and writer parts on the slider, there are more than 40 thin layers of materials forming a TMR device structure. The etching yields of these different materials in the TMR device, such as MgO, IrMn, CoFe, and NiFe were calculated to be able to understand the mechanisms and optimize the processes [7-9]. To gain the best performance of a HDD slider in the plasma etching process, the plasma characterization of an industrial-size ion beam etching (IBE) system were measured and analyzed by using the plasma probe diagnostic method.

In this thesis, the sputtering/etching yields of TMR structure materials in a multilayer thin film of a HDD slider ($Ir_{24}Mn_{76}$, $Ir_{21}Mn_{79}$, MgO, $Co_{90}Fe_{10}$, $Co_{75}Fe_{25}$ and $Ni_{81}Fe_{19}$) were calculated by SRIM package. The initial parameters such as plasma ion types, ion

energy, angles of ion beam and materials - were put in as the staring values in the program. The effects of those parameters were focused on the obtained etching yields along with the energy uses/losses in ion-surface phenomena during an etching process [10]. Then, 2-types of the special plasma probes were made to characterize the plasma characteristics of the IBE system for ABS etching processes. The probes were adjusted into two cases of this etching process; a system with the ion/electron compensation from a plasma bridge neutralizer (PBN) and a system without a PBN. Naturally in IBE system, both ions and electrons are numerously generated. The effects of parameters inputting in the system (an incident angle, a potential difference between grids or a beam voltage, a beam current, and a gas flow in both an ion source and a PBN) were considered from I-V curves. Moreover, the plasma parameters such as floating potential, plasma potential, ion saturation current and ion current density (j_p) in the industrial-size IBE system can be extracted from the plasma I-V characteristic curve. The obtained ion current densities were used to calculate the sputtering/etching rate. Finally, the sputtering/etching rates from the experiments were compared with the simulations.

1.2 Purposes of thesis

จุฬาลงกรณ์มหาวิทยาลัย
CHULALONGKORN UNIVERSITY

1. To characterize the plasma in hard disk drive slider fabrication processes

2. To measure and calculate parameters that affect to ion etching performances of materials in a hard disk drive slider

3. To verify the changes of material properties due to ion bombardments.

1.3 Scope of this thesis

1. Sputtering/etching yields of materials ($Ir_{24}Mn_{76}$, $Ir_{21}Mn_{79}$, MgO, $Co_{90}Fe_{10}$, $Co_{75}Fe_{25}$ and $Ni_{81}Fe_{19}$) were calculated by using SRIM package with input parameters such that ion

energy (450, 550, 750 and 1000 eV), angle of ion beam (0-89 degree with 5 intervals), and plasma ion type (Ar^+).

2. Sputtering/etching rate of each major materials in TMR device were calculated.

3. Special plasma probes were made and installed in the IBE system to characterize the plasma in hard disk drive slider fabrication processes.

4. The simulated results and the experimental results were applied to calculate the etching yields.

1.4 Process of this thesis

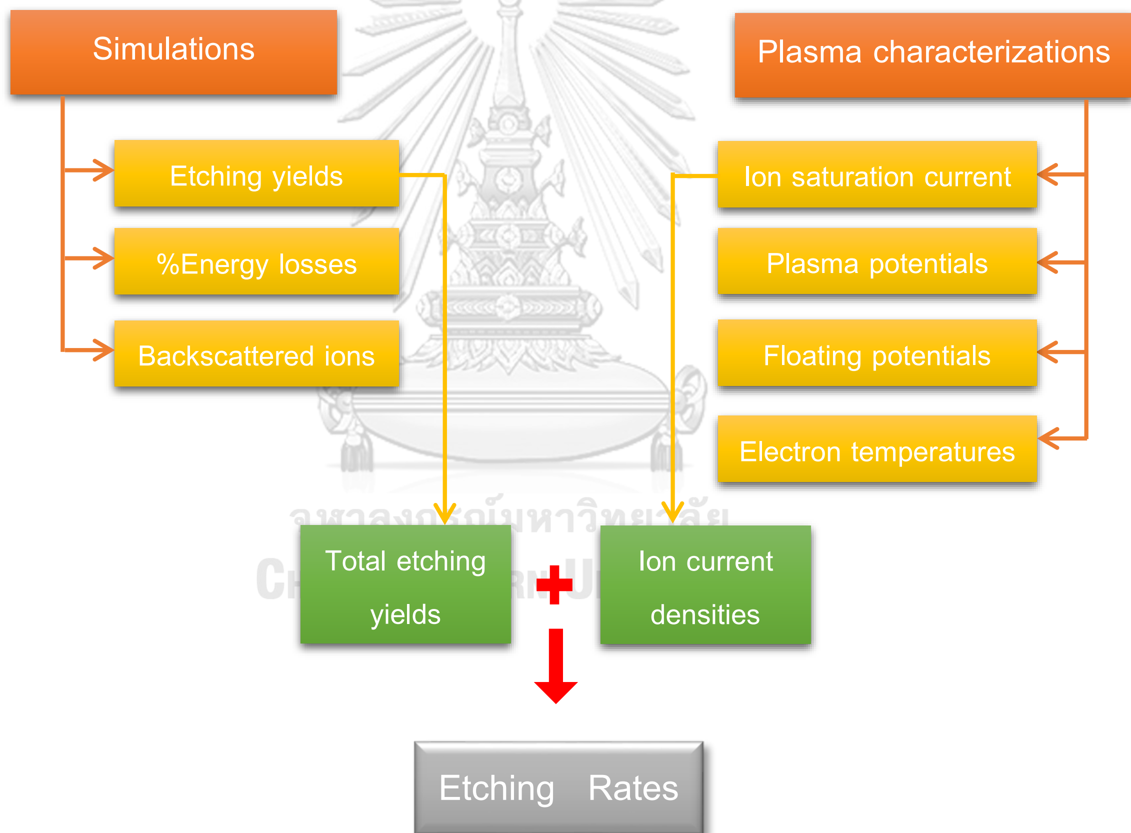

CHAPTER II

THEORETICAL BACKGROUND

2.1 Introduction to Hard Disk Drive (HDD)

A hard disk drive is a permanent data storage hardware used in computers. There are many major components in a HDD, for instance; platters, a spindle, an actuator, a head arm and a read/write head as shown in Figure 1. The platters are a shelf of circular disks which used to be a data storage part. They are made from either aluminium or glass or ceramic which their surfaces are coated with a magnetic material. The platter can rotate with a desired velocity in unit of rpm (revolution per minute) by a control of a spindle motor. The next component is a head arm that can be moved by a small actuator. The head arm is shifted to a parking position when there is no current flow. The last part is a read/write head or slider.

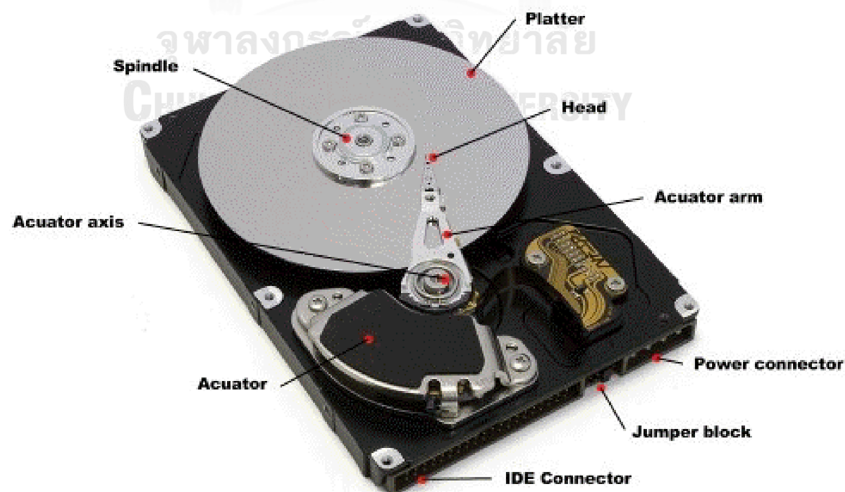

Figure 1 A schematic of components of a hard disk drive [11].

This read/write head is a very tiny part installed at an apex of a head arm as shown in Figure 2(a). The black square is called "slider" which its rim is placed by the actual position of reader and writer that can be seen by a microscope. The slider's function is similar a wing making a head floating above a surface of platters at 5-10 nm height by using the aero dynamic texture underneath the slider, facing down to the media. It is patterned and etched in a specific form called "air bearing surface" or "ABS" (shown in Figure 2(b)). Data reading and writing are done by the sliders moving above the surface of the platters. The HDD sliders transform the platter's magnetic field into electrical currents in the reading process and transform electrical currents into magnetic fields during the writing process [12].

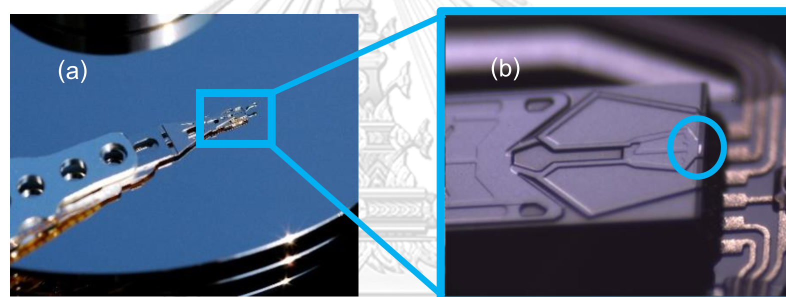

Figure 2 (a) A HDD slider located above a platter, and (b) an ABS under the surface [13]-[14].

จุฬาลงกรณ์มหาวิทยาลัย
Chulalongkorn University

At the edge of HDD slider, there is a tiny thin section made from multilayer thin films of tunneling magnetoresistive (TMR) materials to form a TMR surface, as shown in Figure 3. This TMR device composed of a CoFeB/MgO/CoFeB magnetic tunneling junction (TMJ) is also used in devices such as height-density magnetic recording heads and magnetic random-access memory [9]. Another composition of the HDD slider in a typical example, NiFe/CoFe/Cu/CoFe/Ru/CoFe/PtMn, has CoFe/Ru/CoFe as the synthetic antiferromagnet (SAF) being a pinned layer that is replaced by trilayer structure and consisting of two ferromagnetic layers separated by a thin nonmagnetic interlayer [1].

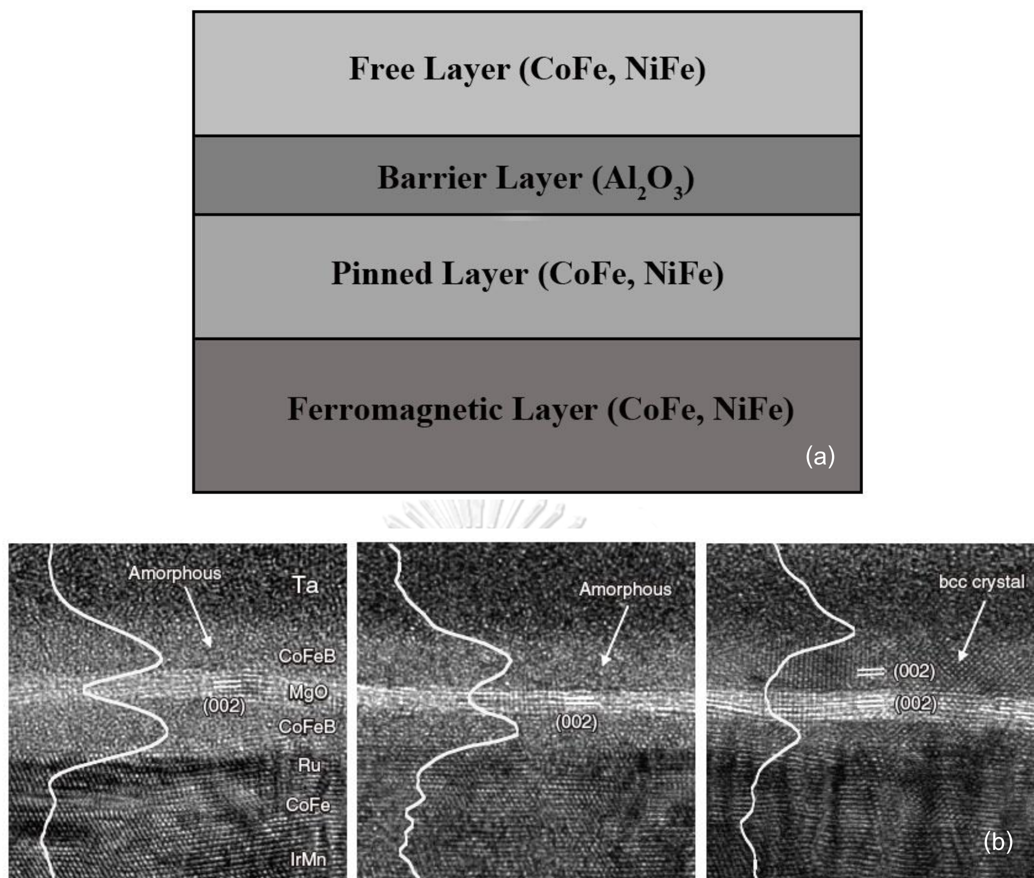

Figure 3 (a) A Schematic of the multilayer stack composition in a HDD slider [8]. (b) A multilayer of TMR device by TEM [9].

จุฬาลงกรณ์มหาวิทยาลัย
Chulalongkorn University

2.2 Basic of plasma

2.2.1 Plasma definition

Plasma is an ionized gas made up of electrons, ions and neutral particles, but electrically neutral. The word was first used by Irving Langmuir in 1928 to describe the ionized gas in an electric discharge. Plasma is sometimes referred as the fourth state of matter [15]. If we continue to increase enough energy to the gas particles, plasma is generated. Since it is common to give temperature in equivalent energy unit (eV), the energy used to generate low temperature plasma should be more than 11600 K (the actual temperature corresponding to 1 eV is 11600 K). Plasma can also be generated by adding the magnetic field in the system. This field results in the electrical interaction of ions and electrons. It has been said that 99% of matter in the universe is in the plasma state (lighting, earth's ionosphere, aurora, earth's magnetosphere, radiation belts, interplanetary medium, solar wind, solar corona, stellar interiors, interstellar medium, laboratory plasmas such as glow discharge, arcs, fluorescent lamps, neon signs, electrical sparks, thermonuclear fusion experiments) [16]. The plasma composition is shown in Table 1 Plasma composition.

จุฬาลงกรณ์มหาวิทยาลัย
Chulalongkorn University

Table 1 Plasma composition

Plasma composition	Density ($1/cm^3$)
Neutral molecules	10^{16}
Radicals	10^{14}
Electrons	10^{8}
Positive ions	10^{8}

From the

Table 1 Plasma composition, the number of radicals is more than ions and electrons a million times. It may be mean that radicals are more formed easily and their lifetime is much longer.

2.2.2 Plasma generation

The plasma can be considered as a sea of neutrals with a small fraction of positive ions and negative electrons. The electrons do not transfer their kinetic energy in the collisions with other molecules, and they can be accelerated with a high energy by the electric field. When energetic electrons collide with neutral molecules, they transfer the energies and momentum to other electrons in the molecules. The collisions can be either elastic or inelastic. Because the mass difference of an electron (m_e = 9.11 x 10^{-31} kg) and a molecule (m_{Ar} = 6.64 x 10^{-20} kg), elastic collisions deplete very little of electron's energy and do not influence the molecules:

$$e^- + Ar \rightarrow e^- + Ar \quad \text{(for elastic collision)}$$

Inelastic collisions excite the gas molecules by completely removing an electron from argon atoms:

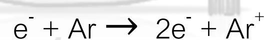

$$e^- + Ar \rightarrow 2e^- + Ar^+$$

จุฬาลงกรณ์มหาวิทยาลัย
Chulalongkorn University

The two free electrons can be accelerated by the field further. This process is called "ionization". It is the most important process that makes other phenomenon occur during that time. There is a reaction which an electron collides with a neutral atom and excites its electron to higher states. This is called "excitation":

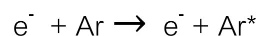

$$e^- + Ar \rightarrow e^- + Ar^*$$

Then, this excited state gas can relax to the ground state by transition and emitting photons. This process is called "glow discharge":

$$Ar^* \rightarrow Ar + h\upsilon \quad \text{(photon that glow)}$$

Those produced electrons are accelerated toward the anode (+) while the positive ions are accelerated toward negative electrode (cathode). The collision between positive ions and the electrode can cause the emission of secondary electrons. All of electrons

are accelerated by the field continuously. Finally, a steady state self-sustaining discharge is obtained. Electrons in a discharge chamber can sometimes be lost by either diffusions into the chamber walls or recombination with positive ions or attachments to neutral molecules to form negative ions:

$e^- + Ar^+ \rightarrow Ar$ (recombination)

$e^- + Ar \rightarrow Ar^-$ (forming a negative ion).

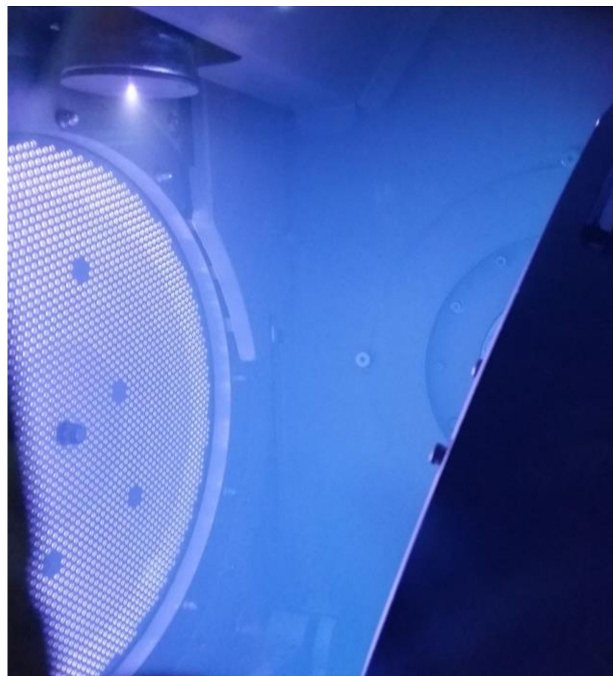

จุฬาลงกรณ์มหาวิทยาลัย
Chulalongkorn University

Figure 4 An argon plasma in IBE system.

2.3 Principle of sputtering/ion etching

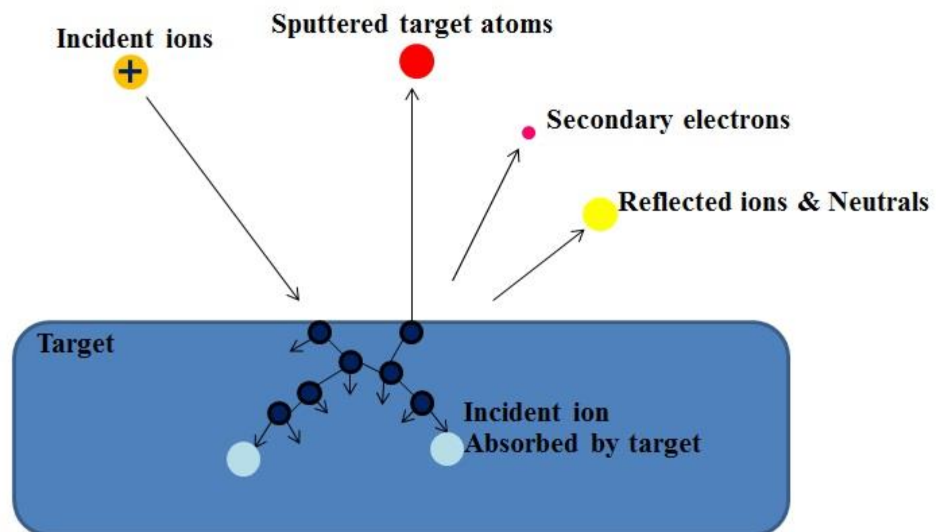

Figure 5 A schematic of sputtering process.

When a surface of any materials is knocked by an energetic ion or a neutral atom, and its energy is more than a surface binding energy, the surface atoms can be ejected. This phenomenon is called “bombardment” or “sputtering” which the momentum and the kinetic energy can be exchanged. The simplest definition of a sputtering process is a process that particles are ejected from a solid target material due to bombardments of the target by energetic particles. The physical sputtering relies on the transfer of kinetic energy and momentum from the incident particles to the surface atoms. Since inert gas, such as argon gas, almost does not react with other atoms and can be accelerated easily under electric fields, regularly, positive ions are used in this process. Typically, there are many processes occurred as ions collide with a surface, which are shown in Figure 5:

- *Reflected ions and neutrals*: As bombardment processes occur, electrons sometimes can leave and recombine with positive ions and then become a neutral atom.
- *Secondary electron emission*: The energetic ions can knock the secondary electrons of the surface atoms.

- *Ion implantation*: If those ions have much energy, they can implant to a surface or it can be called ions absorbed by a target.

2.3.1 Sputtering or Etching yield

A sputtering or etching yield (S) is defined as the ratio between the mean number of atoms removed from the target and an incident ion. It is the measure of the efficiency of sputtering. The sputtering or etching yield can be calculated as a following expression [17]:

$$S = \frac{3\alpha}{4\pi^2} \frac{(4M_i M_t)}{(M_i + M_t)^2} \frac{E_1}{E_b} \cos^2\theta \qquad (1)$$

where α is a monotonic increasing function of M_i/M_t,

E_1 is the energy of incident ions (< 1 keV),

E_b is the binding energy,

M_i is the mass of incident ions

and M_t is the mass of target atoms.

Physical factors which affect a sputtering or etching yield include [18]:

- *Ion energy:*

จุฬาลงกรณ์มหาวิทยาลัย
Chulalongkorn University

There is the energy transformation between bombarded ions and target atoms. The energy of ions should be equal or more than a binding energy of any targets. If the energy increases, the sputtering/etching yield will also increase. The ion implantation can occur if ions have high energy.

Incident ion:

The trend of a sputtering/etching yield depends on the atomic number of an incident ion. The highest yields occur when the mass of incident ion match with the mass of the target materials.

- *Angle of incident ion beam:*

The sputtering/etching yield also depends on an angle of incident ion beam, which is the angle between a normal line and a surface of target. The maximum value is given at the angle of 60 degree approximately.

- *The ion flux (ion current):*

  Increasing in the ion flux influences an increasing in the number of ejected atoms.

2.3.2 Sputtering or etching rate calculations

The sputtering or etching rate is the number of target atoms removed per a unit of time. This rate of each material in Å/min can be calculated following in the expression:

$$\text{Sputtering / Etching rate} = 62.2\frac{M}{\rho}Sj_p \qquad (2)$$

where M is a molar weight of the target [g/mol],

ρ is a density of the material [g/cm^3]

and j_p is a primary ion current density [mA/cm^2].

For an example in a calculation of Si target (S = 0.45 atoms /ion for 500 eV of argon ions at normal incident), it gives the sputtering rate of 340 Å/min for an ion current density of 1 mA/cm^2 [19]. In the equation (2), it indicates that the etching rate depends on many factors. If the target material is specified, the etching rate depends only on a primary ion current density. In this work, if the ion current density can be calculated from an I-V curve, the etching rate of our materials in this industrial-size IBE system can be known.

จุฬาลงกรณ์มหาวิทยาลัย
CHULALONGKORN UNIVERSITY

2.4 Ion Beam Etching (IBE)

In fabrication of many electronic devices, techniques being controllable manner are essential. The steps that the materials are removed from the surface of a desired region in the sample is called etching [20]. Sometimes there is a mask which is used to

protect the desired regions of the wafer surface. The unprotected materials are etched from the surface of target. Example of mask is a photoresist. There are two main etching techniques which are wet etching and dry etching processes. For wet etching process, liquid chemicals (etchant) are used, usually acid-based solutions. The surface atoms are etched by the chemical reactions or by the dissolutions. The reaction products must be soluble in etchant solution. In contrast, dry etching process employs plasma of gas. The materials are removed by the chemical and/or physical reaction. The products from the reactions may be volatile and carried away in the gas stream. Ion beam etching (IBE) technique is the dry etching process which is the important and well known technique in fabrication of most electronic devices. The advantages of IBE are that it provides a good control of both a structural size and shape, even on a sub-micron scale and at low process temperature [21]. Other advantages of this dry etching process -especially IBE process – are that there is no photoresist adhesion problems, anisotropic etch profile is possible as shown in Figure 6(b), chemical consumption is small, a disposal of reaction products less costly and suitable for automation. The anisotropic profile is defined as the profile with the directional etching - the film is not etched under the mask.

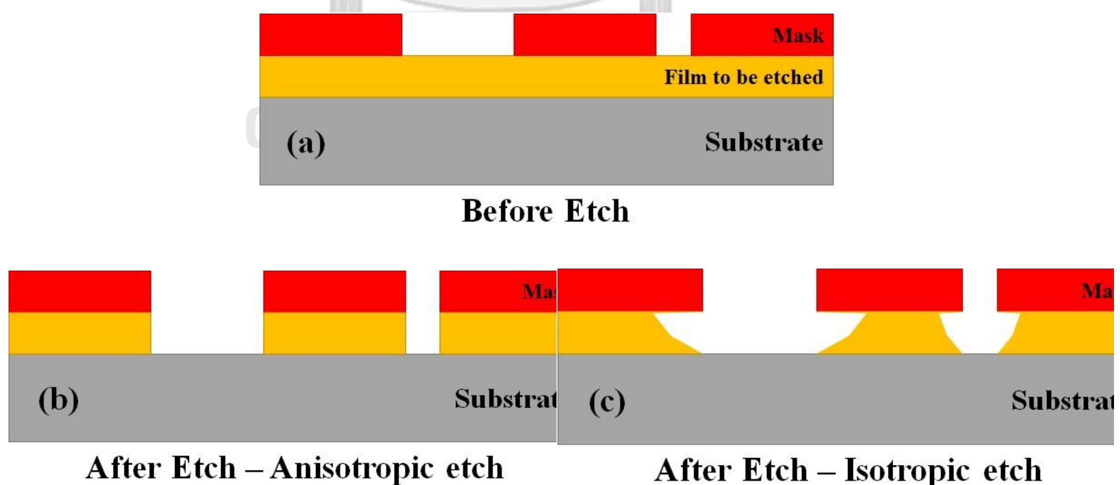

Figure 6 Directionality of etching.

IBE which is used to fabricate electronic devices employs a broad beam area ion source to direct an energetic beam of a noble gas, such as Ar, Xe, Ne or Kr, to remove materials by physical sputtering [22]. The IBE system consists of 3 main parts: an ion source, ion-optic grids and a plasma bridge neutralizer (PBN). An ion source is a plasma source having a set of ion-optic grids that enable extraction of a stream of ions. The ion-optic grids are served to determine the energy of the incident ion beam and angular divergence of the ions within the beam. PBN is the electron source that is used to balance the net charge in the beam and to prevent charging of the target surface.

2.4.1 Ion source

Ion production is done in the discharge chamber by subjecting a gas to an energy field. Free electrons are excited by the field until they have enough energy to break gas molecules into ions and electrons that can further ionize gas molecules ensuring that the gas is thus ionized and plasma is established. The ion source generates a low temperature plasma with slow (cold) ions and low ion temperature. These energetic ions can be extracted with a well-defined energy.

The energetic electrons collide with gas molecules and create new species. There are many collision processes occurring in an ion source:

- *Ionization*: electrons are removed from gas molecules or atoms and then positive ions exist simultaneously.
- *Electronic excitation*: when the free energetic electrons transfer the energy to other electrons in gas molecules, they excite some those electrons to higher

energy levels. When they fall back to lower levels, they emit energy usually in the form of photons of visible light.

- *Molecular fragmentation*: the collision of electrons and molecules makes the fragmented, resulting in unsatisfied bonding which is chemically reactive. These usually are called radicals.
- *Radicals*: they have no net charge. So they cannot be accelerated or cannot be attracted by any fields or any charge particles, respectively. Their lifetimes are long when are compared to others.

จุฬาลงกรณ์มหาวิทยาลัย
CHULALONGKORN UNIVERSITY

2.4.2 Ion-optic grids

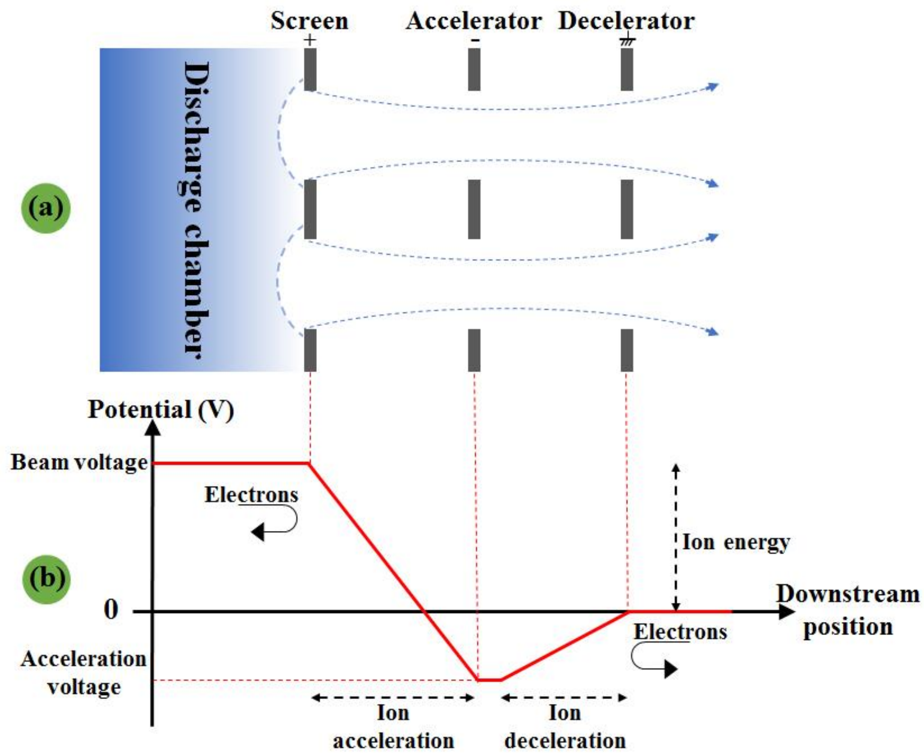

Figure 7 (a) A schematic of the set of ion-optic grids and (b) their final energy of the accelerated ions.

จุฬาลงกรณ์มหาวิทยาลัย
Chulalongkorn University

The set of the grids has important roles for extraction and acceleration of ions to the required energy. This set of grids consists of three grids as shown in Figure 7(a), which has a specific hole pattern with several apertures forming beamlets. A combination of all these individual beamlets then forms the broad ion beam. Grid curvature and inter-grid separation are also significant design features which depend on the application required, for example depending on the target size to be sputtered for deposition or substrate size and etch rate for etch applications. In a grid system, specific potentials or voltages applied between the first two grids provide the driving force for the ions. The inner grid in contact with the plasma, known as the “screen grid”, is the one that determines the beam voltage or energy. This is biased a positive potential relative to ground. The second - “accelerator” grid - is biased negative with respect to the ground, and offers the extraction voltage, which is the potential difference for the beam ions. The last grid - “decelerator”

grid - is normally grounded and helps beam collimation reducing divergence of the beam, minimizes electron back-streaming and re-deposition of sputtered material back onto the accelerator grid. The final energy of the accelerated ions is equal to the set beam energy or voltage (V_B), as shown in Figure 7(b). It shows that the final ion energy depends on the potential of the screen grid with respect to the ground.

2.4.3 Plasma bridge neutralizer (PBN)

The third element in IBE system is a plasma bridge neutralizer or PBN which is basically an electron source. It is usually located in the etching chamber between the ion-optic grids and the sample holder illustrated in Figure 8. Normally, the PBN is not used in the general sputtering system [23]. In this IBE system, since the grids confine electrons into the generator chamber, the electrons in the etching chamber is rare. The purpose of this PBN is to balance the charge of the ions in the beam in order to reduce space-charge effects causing beam divergence through mutual repulsion of the ions and to prevent charging of the target surface. The PBN is not used to form neutral atoms within the beam, but to eliminate any net charge of atoms within a given volume of the etching beam. The electrons provided by the PBN do not reenter the grid set due to the negative potential on the accelerator grid.

CHULALONGKORN UNIVERSITY

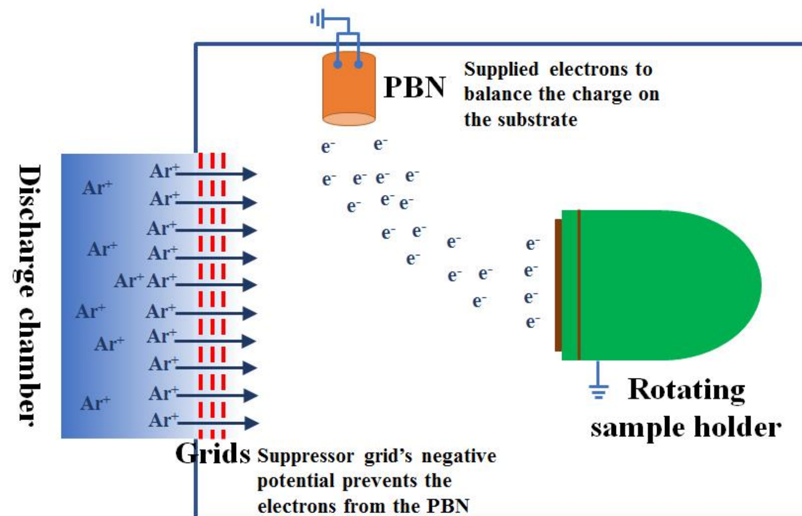

Figure 8 An industrial-size IBE system with the ions/electrons compensation by a PBN.

2.5 Plasma characterization

2.5.1 Plasma probes

Figure 9 Langmuir probe [24].

The device used to diagnose the electron temperature, electron density and the plasma potential is called "plasma probe" or "Langmuir probe" as shown in Figure 9. Its name was obtained after Nobel Prize winning physicist Irving Langmuir. The plasma

จุฬาลงกรณ์มหาวิทยาลัย CHULALONGKORN UNIVERSITY

characterization by Langmuir probe can be done by inserting an electrode into the plasma and electrically biasing with respect to a reference electrode to collect electrons and/or positive ion current. For a single plasma probe, the current (I) collected to a small disc inside the plasma is given as:

$$I = A\sum_{i=1}^{N} n_i q_i \bar{v}_i \qquad (3)$$

where A is the total collecting area of the surface of the flat probe that is given by $A = \pi r^2$ and n_i is the number of species with their charges q_i. $\bar{v}_i$ is the average velocity of species:

$$\bar{v} = \left(\frac{1}{n}\right)\int v f_i(\bar{v})d\bar{v} \qquad (4)$$

In the equilibrium, the velocity distribution function f_i or Maxwellian distribution for each species i is shown as [25]:

$$f_i(\bar{v}) = \left(\frac{2\pi kT_i}{m_i}\right)^{-\frac{3}{2}} \exp\left(\frac{-\frac{1}{2}m_i(\bar{v})^2}{kT_i}\right) \qquad (5)$$

The plane of disc probe is considered and defined it in the y-z plane. A particle gives the current only if it has the same component of velocity – v_x. The current to the probe thus does not depend on the y and z-component of velocity. The current from each species (electron or ion) can be written as:

$$I = nqA\bar{v}_y\bar{v}_z\left[\int_{v_{min}}^{\infty} v_x\left(\frac{2\pi kT_i}{m_i}\right)^{-\frac{1}{2}} \exp\left(\frac{-\frac{1}{2}m_i v_x^2}{kT_i}\right)dv_x\right] \qquad (6)$$

where $\bar{v}_j = \int_{-\infty}^{\infty}\left(\frac{2\pi kT_i}{m_i}\right)^{-\frac{1}{2}} \exp\left(\frac{-\frac{1}{2}m_i v_j^2}{kT_i}\right)dv_j$; j is y and z. Particles with x-component of velocity less than v_{min} are repelled.

$$V_{min} = \sqrt{\frac{2qV}{m_i}} \qquad (7)$$

Integrals of y and z components of velocity give a unit, then the total current of each species to the probe will be:

$$I(v_x) = nqA\left[\int_{v_{min}}^{\infty} v_x \left(\frac{2\pi kT_i}{m_i}\right)^{-\frac{1}{2}} \exp\left(\frac{-\frac{1}{2}m_i v_x^2}{kT_i}\right) dv_x\right] \tag{8}$$

2.6 Plasma characteristics

From plasma probe measurement, the data can be analysed as a plot of I-V characteristics of plasma. The information about the plasma characteristics in the IBE system are extracted and discussed in this section.

2.6.1 Ion currents to the probe

When the bias potential V_{bias} on the probe is enough negative with respect to the plasma potential (V_p), the ion saturation current I_{is} is collected (the range of $V_{bias} \in (-\infty, A)$ in Figure 10 The ideal I-V curve.). It continues to be collected until the probe bias voltage reaches V_p. At this point, ions begin to be repelled. For $V_{bias} >> V_p$, all positive ions are repelled and ion current vanishes. For a Maxwellian ion distribution, the ion current $I_i(V_{bias})$ on V_{bias} is given by:

CHULALONGKORN UNIVERSITY

$$I_i(V_{bias}) = \begin{cases} -I_{is}\exp\left[\dfrac{e(V_p - V_{bias})}{kT_i}\right] & ;V_{bias} \leq V_p \\ -I_{is} & ;V_{bias} \leq V_p \end{cases} \tag{9}$$

where e is the charge of electron and k is the Boltzman constant. When T_i is comparable to the electron temperature T_e, the ion saturation current is given by:

$$I_{is} = \frac{1}{4} e n_i v_{i,th} A_{probe} \tag{10}$$

where n_i is the ion density, $v_{i,th} = \sqrt{8kT_i / \pi m_i}$ is the ion thermal velocity. The fact that the ion current is defined by the electron temperature occurs when T_e is much greater than T_i, thus the ion saturation current is determined by the Bohm ion current [26]

$$I_{is} = I_{Bohm} = 0.6en_i \sqrt{\frac{kT_e}{m_i}} A_{probe} \tag{11}$$

2.6.2 Electron current to the probe

From the previous section, all electrons are repelled for $V_{bias} << V_P$ so that $I_e = 0$ but there are some electrons which are collected by the probe if $V_{bias} < V_P$. In the Maxwellian electron velocity distribution, the electron current increases with increasing potential exponentially. As the probe potential V_{bias} is much more than the plasma potential V_P, there are only electrons move to the probe causing the electron saturation current I_{es} occurs (the range of $V_{bias} \in (V_P, \infty)$ in Figure 10 The ideal I-V curve.). The electron current can be written in the function of V_{bias} as:

$$I_e(V_{bias}) = \begin{cases} -I_{es}\exp\left[\dfrac{-e(V_p - V_{bias})}{kT_e}\right] & ;V_{bias} \leq V_p \\ -I_{es} & ;V_{bias} \leq V_p \end{cases} \tag{12}$$

The electron saturation current I_{es} is:

$$I_{es} = \frac{1}{4} en_e v_{e,th} A_{probe} \tag{13}$$

where n_e is the electron density, the electron thermal velocity is $v_{e,th} = \sqrt{8kT_e / \pi m_e}$ and electron with the mass m_e.

จุฬาลงกรณ์มหาวิทยาลัย
CHULALONGKORN UNIVERSITY

2.6.3 I-V characteristic

When the probe is biased negative and positive potentials with respect to the ground, the current from electrons and/or positive ions can be measured, as described before. The I-V curve can be plotted between the bias potential versus the measured ion and ion currents, as shown in the

Figure 10 Note that, the current in the probe which is obtained is the total current $I(V_{bias}) = I_e(V_{bias}) + I_i(V_{bias})$.

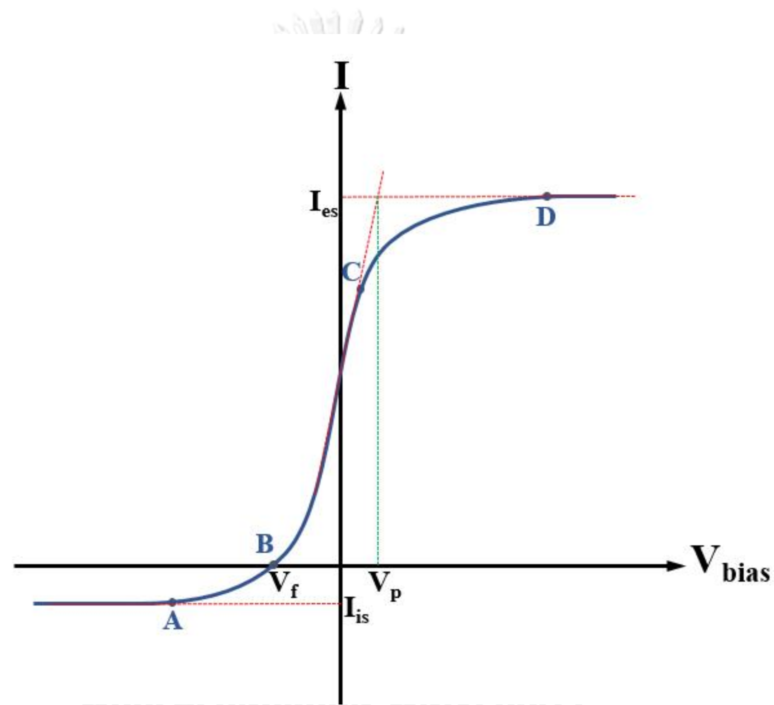

Figure 10 The ideal I-V curve.

- *Region A – B*: Most of electrons are repelled from the probe while the positive ions are attracted to the probe. There is only ion current when the biased potential is more negative until the ion saturation current I_{is} is occurred. Electrons can toward to the probe causing the electron current occurs when the bias potential is increased. The bias potential is the floating potential V_f where the contributions of the ion and electron currents are equal (I_{probe} = 0).

- *Region B – C*: In this transition region (V_f < V_{probe} < V_p), the probe will only collect electrons having kinetic energy more than the value of $e|V_{probe} - V_p|$. In the Maxwellian plasma, this region of the curve is exponential.
- *Region C – D*: For a more positive bias potential, all of ions are repelled while the electrons are the attracted charges by the probe. Electrons are responsible for the electric shielding of the probe called the *electron saturation current* I_{es} in this case.

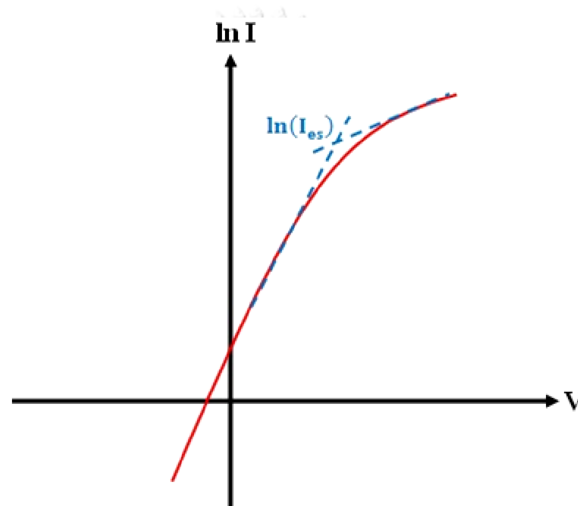

Figure 11 A plot of ln|I| versus a bias potential.

จุฬาลงกรณ์มหาวิทยาลัย
Chulalongkorn University

Moreover, the electron temperature of the plasma can refer to an energy transfer which occurs from the collision of electrons can be analysed from this curve. The I-V curve will be plotted to the curve of a ln|I| versus a bias potential as shown in the Figure 11. The electron temperature can be calculated from the slope of this plot from its linear part, using equation (9),

$$\left|I_e(V_{bias})\right| = I_{es}\exp\left[\frac{-e(V_p - V_{bias})}{kT_e}\right] \tag{14}$$

$$\ln\left|I_e(V_{bias})\right| = \ln(I_{es}) - \frac{e(V_p - V_{bias})}{kT_e} \tag{15}$$

Since the I_{es} is the constant, the derivative of $\ln\left|I_e(V_{bias})\right|$ with respect to V_{bias} will be:

$$\frac{d\ln\left|I_e(V_{bias})\right|e}{dV_{bias}} = \frac{e}{kT_e} \tag{16}$$

$$\text{Slope} = \frac{e}{kT_e} \tag{17}$$

The above equation shows that the slope of the ln|I|-V plot is the inverse of the electron temperature in the unit of electron volt (eV). Sometimes the floating potential can be calculated from an equation (6) with the fact that $I(V_{bias}) = I_e(V_{bias}) + I_i(V_{bias})$.

$$I(V) = I_{is} - neA\left[\left(\frac{kT_e}{2\pi m_e}\right)^{\frac{1}{2}} \exp\left(\frac{-eV}{kT_e}\right)\right] \tag{18}$$

This means that the slope of plasma I-V curve determine electrons collision in the system.

Another important parameter in the plasma characterization is the ion current density, j_{ion}. This value indicates the ratio between the number of ions that forward to a probe and an area of the probe. It can be used to calculate fir the sputtering/etching rate and the ions to neutral arrival rate ratio. The ion current density is calculated by the expression:

จุฬาลงกรณ์มหาวิทยาลัย
Chulalongkorn University

$$J_{ion} = \frac{I_{probe}}{V_{probe}}[A/m^2] \tag{19}$$

$$J_{ion} = \frac{(6.24\text{x}10^{15})I_{probe}}{V_{probe}}[ions/m^2]. \tag{20}$$

2.7 Concept of simulation

The Stopping and Range of Ions in Matter (SRIM) package is a group of programs that is used to calculate the stopping and range of ions into matter in this work. The statistical method – Monte Carlo – is used as a basic for this calculation. As the ions collide with atoms of matter, many phenomena can be occurred. Some of these phenomena are the creation of vacancies by ion collisions and recoiling atoms. As the example shown in Figure 12, the phosphorus ions with their tracks (red dots) knock a silicon matter away from their lattice sites – vacancy creations. The green dots are the vacancies which are occurred by the recoiling silicon atoms [27]. The recoil atom is defined as the atom in matter that is moved out from its lattice site and it can collide with other atoms further. Every time there is a target/ion collision, and a green dot is formed, there is an opportunity that the ions change their directions.

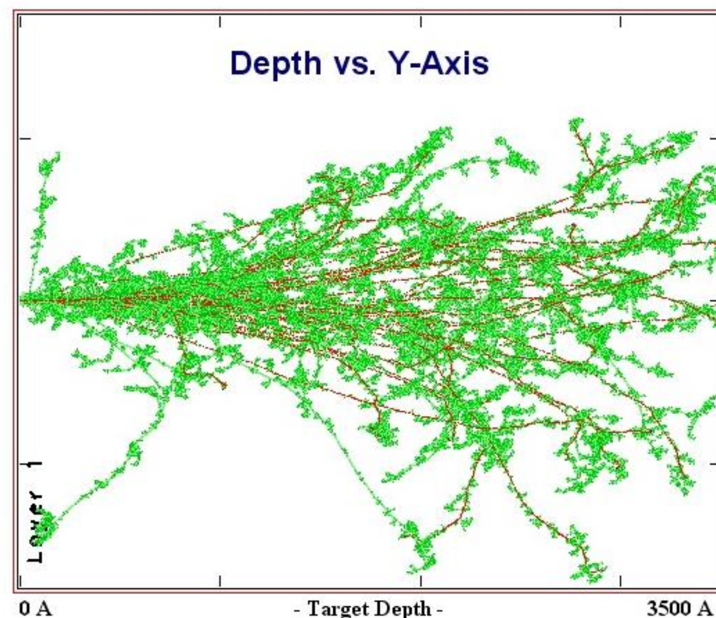

Figure 12 The paths of phosphorus ions that are hitting a silicon material [27].

Since the mass of phosphorus and silicon are almost the same, the phosphorus ion can transfer more of its energy to silicon atom. Thus the ions can deeply penetrate into the matter.

In Figure 13, the argon ions (light mass) collide with the $Ni_{81}Fe_{19}$ target (heavy mass). If the mass of ion/target atoms are very different, there is the less energy that can transfer to the target atoms. So the ions penetrate near the surface of the target as see in Figure 13(a). This is the basic physics of the elastic collision, which both momentum and kinetic energy are conserved.

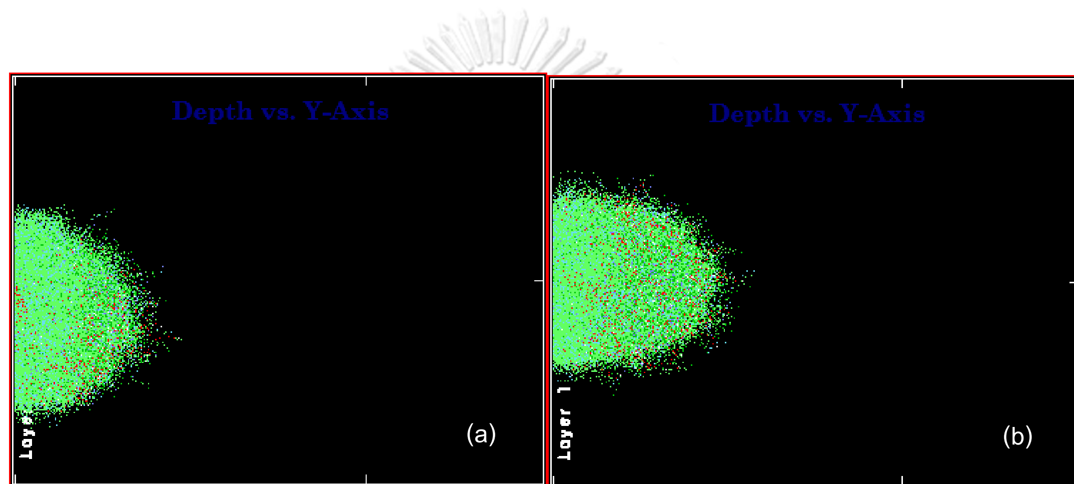

Figure 13 The argon ions which penetrate near the surface of $Ni_{81}Fe_{19}$ target at the ion incident angle of (a) 75° and (b) 0° (normal to the surface of a target).

CHULALONGKORN UNIVERSITY

Moreover, the direction of incident ions causes the direction of ions in the matter including of the occurring recoil atoms. As shown in Figure 13(a), the argon ions come from the top with the angle of 75° the normal surface. The ion penetration into the $Ni_{81}Fe_{19}$ target is shallower than for the angle of 0° (normal to the surface), as shown in Figure 13(b).

CHAPTER III

SIMULATIONS AND EXPERIMENTS

3.1 Plasma etching simulation

In this work, we used the Monte Carlo-based simulation package – SRIM (the stopping and range of ions in matter written by James F. Ziegler) to simulate an etching behavior and to calculate etching yields of some important layer materials within TMR structure of HDD slider. The parameters such as; plasma ion types, energy of ions, incident angle and composition of target material, were input into the software. We focused on the effect of those parameters to the obtained sputtering yields at different condition, according to the actual processes, as shown in Table 2. The procedures of simulation will be explained as the following.

Table 2 The conditions of input parameters.

Plasma ion types	Argon ion (Ar^+)
Ion Energy (eV)	450, 550, 750 and 1,000
Incident angle	0°-89° with 5 intervals
Target materials	$Ir_{24}Mn_{76}$, $Ir_{21}Mn_{79}$, MgO, $Co_{90}Fe_{10}$, $Co_{75}Fe_{25}$ and $Ni_{81}Fe_{19}$

In calculations, we simulated the ions collide with each monolayer of the target material. For an example of each simulation, the argon ions were chosen to etch the $Ir_{24}Mn_{76}$ specimen with 450 eV and its angle was set at 0° (normal to the surface plane). In our calculations, we simulated about 100,000 of argon (Ar) gas molecules accelerated toward the surface of target materials.

จุฬาลงกรณ์มหาวิทยาลัย
Chulalongkorn University

After those parameters were input and then the simulation was started, the software showed both the ion behaviour in the specimen and the calculated output parameters – sputtering yields of each element, % energy losses and backscattered ions. The front interface of the simulation program was shown in Figure 14.

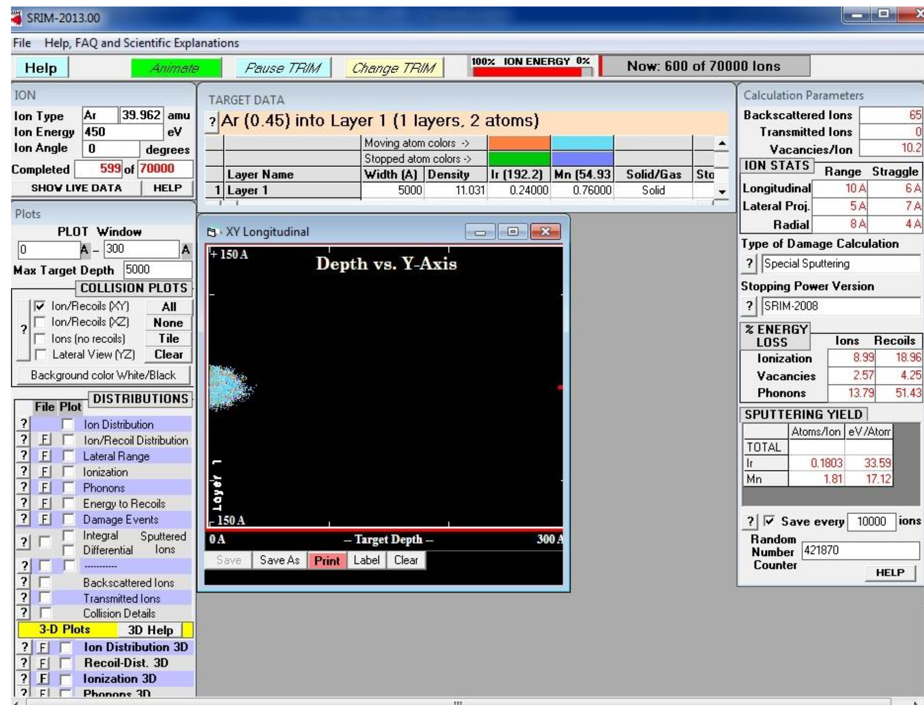

Figure 14 Simulation interface panel.

จุฬาลงกรณ์มหาวิทยาลัย
CHULALONGKORN UNIVERSITY

After the simulation was completed, the sputtering yield for each element of the compound materials was obtained. Other etching parameters related to the ion bombardment products were also calculated, such as backscattered ions and % energy losses.

% ENERGY LOSS	Ions	Recoils
Ionization	8.99	18.96
Vacancies	2.57	4.25
Phonons	13.79	51.43

Figure 15 The percentage of energy loss during simulation.

The energy of ions and recoil atoms can be lost to cause ionizations, vacancies, including phonons (phonon is the energy stored in atomic vibrations in a crystal). Ionization is the energy loss to the target electrons. The energy of ions and recoil atoms are absorbed by the electrons in the target and then they are released as heat if the target is metal, or as phonons if the target is an insulator. Figure 15 showed the products from the incident ion energy into various types. For example, the ions generated phonons with 13.79% of their incident energy of 450 eV together with the recoil atoms generated an additional 51.43% = 65.22% (total). Thus, the energy was about 65.22% x 450 eV = 293.49 eV of phonons per incident ion [27].

3.2 Experimental details on plasma characterization

จุฬาลงกรณ์มหาวิทยาลัย
CHULALONGKORN UNIVERSITY

In this work, the Veeco Nexus IBE350 IBE system was used to study the plasma characteristics. This was the same system which had been used in the HDD production line. The based pressure of this industrial-size ion beam etching system was pumped to 3.8×10^{-7} torr. To measure the plasma I-V curve, the plasma probes were installed at an actual specimen holder position inside the main vacuum chamber, shown in Figure 16(a). Normally, the plasma flat disc probe was suitable for measuring the ion current while the wire-type probe was for electron measurement [17]. Both of them were made from metal and were connected by a copper cable with a ceramic sheath to a circuit outside the vacuum chamber illustrated in Figure 16(b).

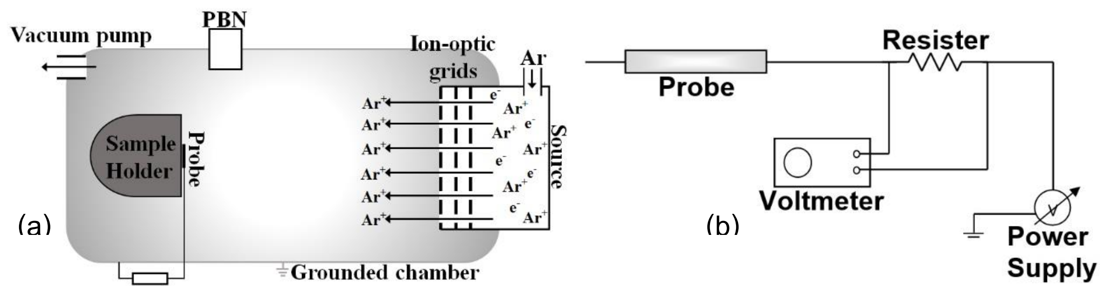

Figure 16 (a) A schematic representation of the experimental setup. (b) A schematic representation of the special flat/wire plasma probe's circuit.

In the fabrication process, argon ions were accelerated - from a source through a set of ion-optic grids and eventually hit the surface of materials. In order to characterize ions and electrons that reached the target surface, both probes were placed at the specimen's position. Those probes were then biased a sweep potential – vary from negative to positive respect to ground. The I-V curves in any desired conditions were plotted from the measured data – measured current versus bias potential. The incident angles were varied as +20°, 0° (normal to the surface) and -30° as shown in Figure 17. Next parameter was the beam voltage in this system, which was the potential difference between a screen grid and a ground aimed to extract the ions. The kinetic energy of ions was determined by this potential. Both the beam current – current that was applied to generate the plasma - and beam voltage were set as 400, 600, 800 mA and 400, 600, 800 volts respectively.

จุฬาลงกรณ์มหาวิทยาลัย
CHULALONGKORN UNIVERSITY

Other two parameters causing the changes in this system were the gas flow in PBN and ion source. The argon gas was fed to PBN unit. The PBN is the electron source in IBE system to generate free electrons. The rate flow of an argon gas into PBN was varied at 4, 6 and 8 sccm (Standard Cubic Centimeters per Minute). The last parameter was the argon gas that was flowed into an ion source to generate the plasma. A flow rate determined the number of ions in chamber before picking out to an operating chamber by grids. This argon flow rate in this work was varied to 16, 20 and 24 sccm, respectively.

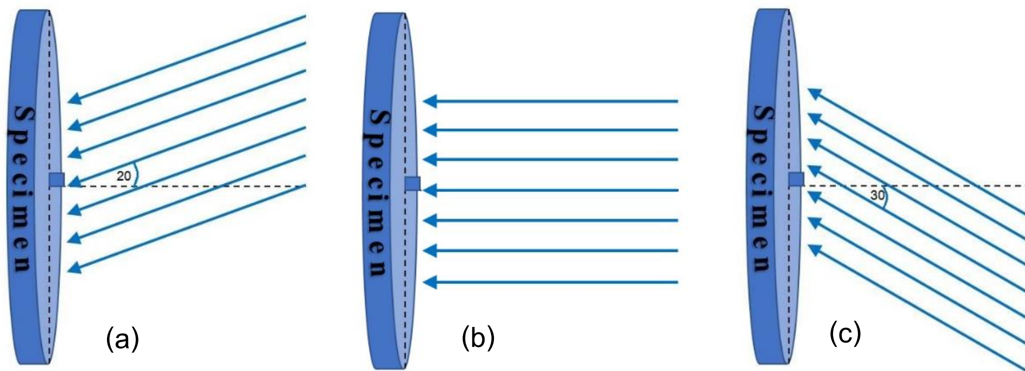

Figure 17 The definition of the incident beam directions though out from grids – (a) +20°, (b) 0° (normal to the surface) and (c) -30°.

For negative and positive angle, they can be implied that they are almost the same angle such as +20° is almost equal to -30°. The difference of each is just the direction of an incident beam which ions come from the top and bottom for positive and negative way respectively. Because of the actual process, these angles were chosen to study. The different ABS pattern depends on the different etching angle. Moreover, the wall angle of ABS pattern needed these angles to be etched in this process.

จุฬาลงกรณ์มหาวิทยาลัย
Chulalongkorn University

3.2.1 Experimental design

The bias voltage from a power supply was biased (from -14 volts to 14 volts) to the probe during the measurement. After that the voltage that through the fixed value resistor were measured to calculate the plasma current. The range -14 to 0 volts were biased and measured by a wire probe and the remaining range by a flat probe.

CHAPTER IV

RESULTS AND DISCUSSION

4.1 Etching yield simulations

From the SRIM calculations, the plots of the etching yield versus angle of incident for 4 different kinetic energies of argon ions were shown from Figure 18 to Figure 23 for 4 different materials in TMR structure ($Co_{90}Fe_{10}$, $Co_{75}Fe_{25}$, $Ni_{81}Fe_{19}$, $Ir_{24}Mn_{76}$, $Ir_{21}Mn_{79}$ and MgO). All of these materials were classified as the ferromagnetic material (CoFe and NiFe), antiferromagnetic material (IrMn) and insulator (MgO).

The results showed the same trends for all materials. The etching yield of those materials increased with ion impact angle - and reached a maximum yield around 60º - 70º to the surface plane before dropped down as it gets close to 90º. It can be noticed that the angles for each maximum yield were increasing, following the energy of ions. This may be resulted from the penetration of the energetic ions. The ions with high energies can more penetrate into the surface of materials than the ions with low energies. The highest etching yield from the collision of energetic ions was about the angles between 60º - 70º. The atomic ratio of elements which was the composition of binary alloy compounds affected to the values of the etching yields of them directly. The etching yields of Co, Ni and Mn which was the main elemental composition of each binary alloy compound was more than the Fe, Fe and Ir, respectively. The dependence of elemental ratio in the compound was clearly observed in the yield of CoFe alloy materials, as shown in Figure 18 and Figure 19. If the atomic ratio of the Co and Fe was close each other, the etching yield value of each material was shifted toward each other, as shown in Figure 19. On the other hand, the value of etching yields will be much different if the atomic ratio is more different. For the equivalent ratio of atoms in a unit cell of the compound, such as

จุฬาลงกรณ์มหาวิทยาลัย
CHULALONGKORN UNIVERSITY

MgO shown in Figure 21, the etching yield of each element was not almost different. Since the atomic numbers of Mg and O were closed, their etching yields were also closed. Moreover, the incident ion energy can help to increase the etching yield as well. As the energetic ions collide with the surface atoms, their energies are transformed those atoms. The incident ions with much energy can transfer more their energy. The surface atoms will be much released.

The right y-axis of the Figure 18, Figure ***19*** and Figure ***20*** was the number of backscattered ions that was created from the etching phenomena, as a function of incident angle. The percentage of incident ions that transformed to backscattered ions was getting higher as the incident angle approaches 90°. As the ions impacted on the surface of a target at the normal angle (0°), those ions had more penetration depth into the target material. The number of backscattered ions was increased continuously as the incident ion angle increased. Therefore, in order to decrease the number of backscattered ions in production process, the incident angle of bombarded ion was set at about 65°.

จุฬาลงกรณ์มหาวิทยาลัย
Chulalongkorn University

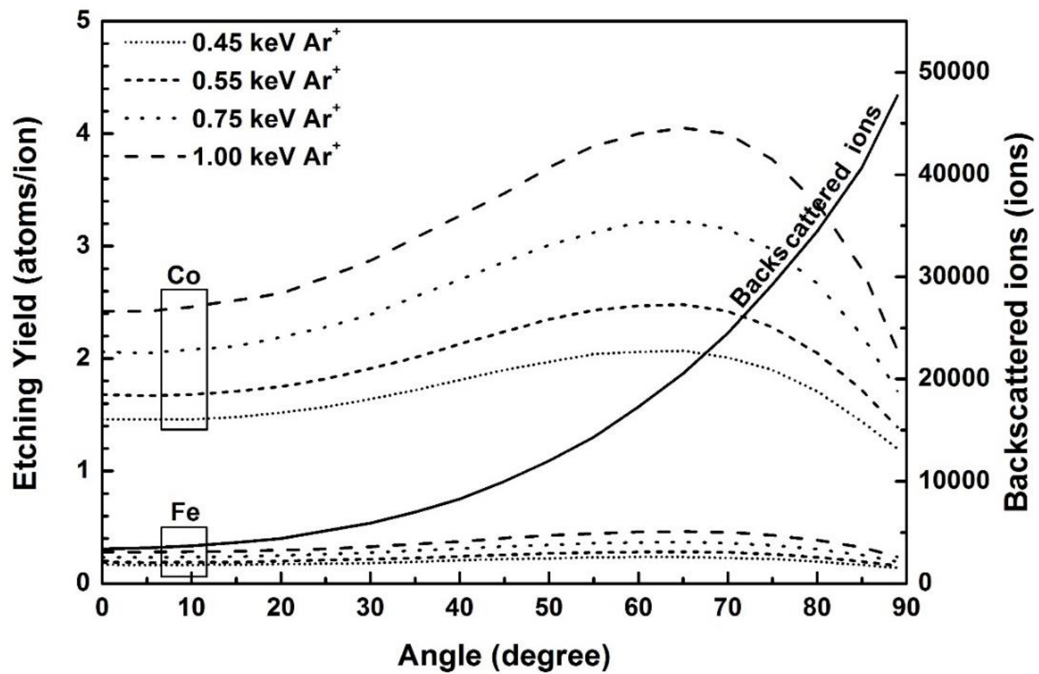

Figure 18 Plots of the calculated etching yields and backscattered ions versus angle of the argon ions incident on $Co_{90}Fe_{10}$ material using SRIM.

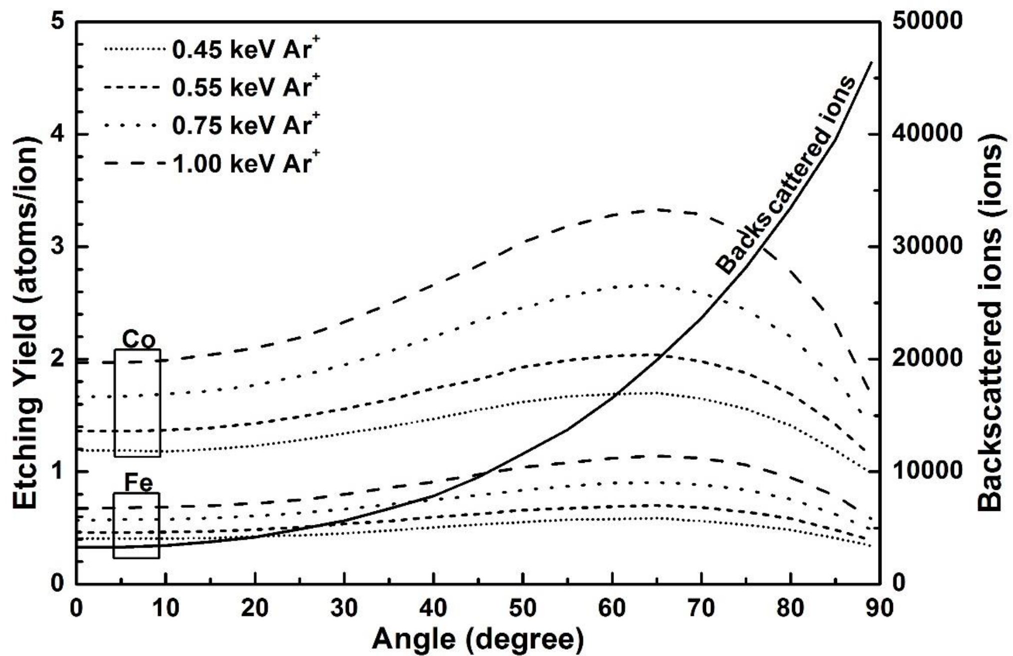

Figure 19 Plots of the calculated etching yields and backscattered ions versus angle of the argon ions incident on $Co_{75}Fe_{25}$ material using SRIM.

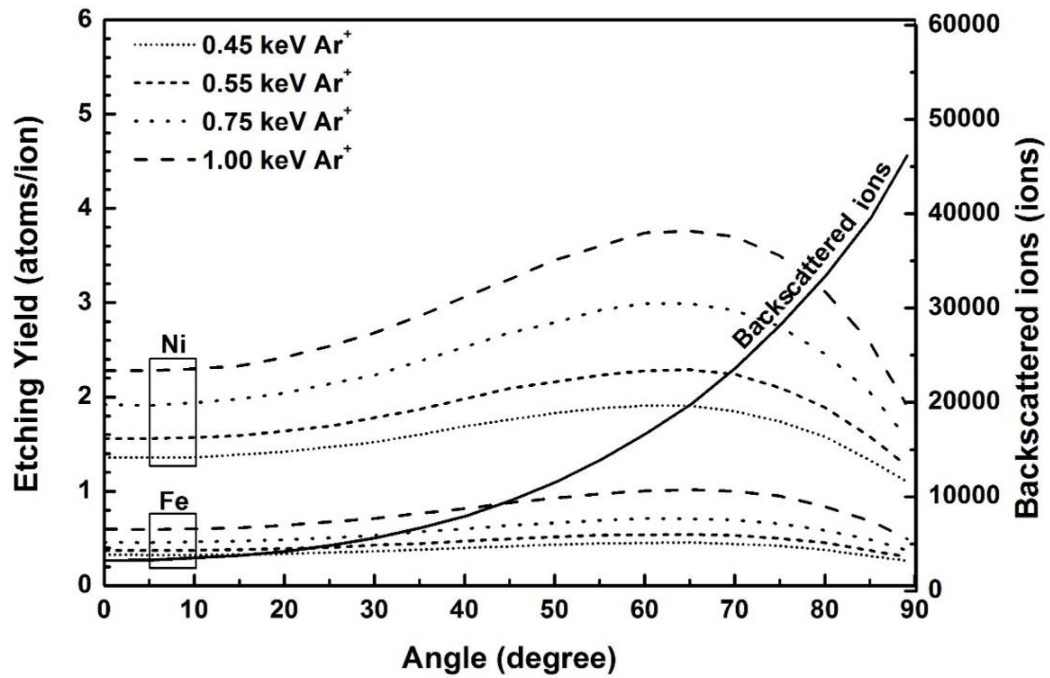

Figure 20 Plots of the calculated etching yields and backscattered ions versus angle of the argon ions incident on $Ni_{81}Fe_{19}$ material using SRIM.

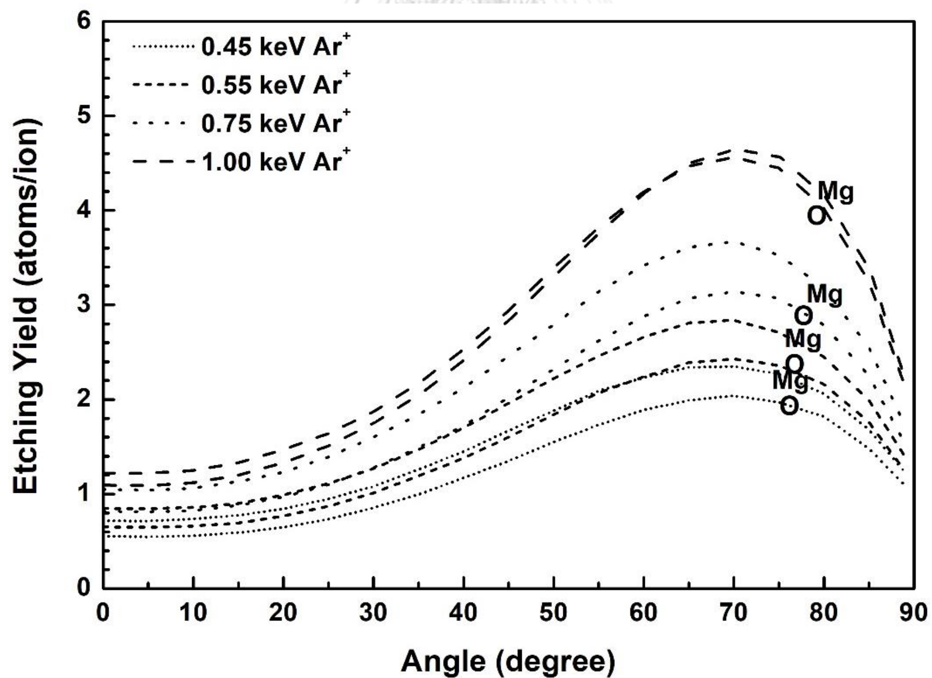

Figure 21 Plots of the calculated etching yields versus angle of the argon ions incident on MgO material using SRIM.

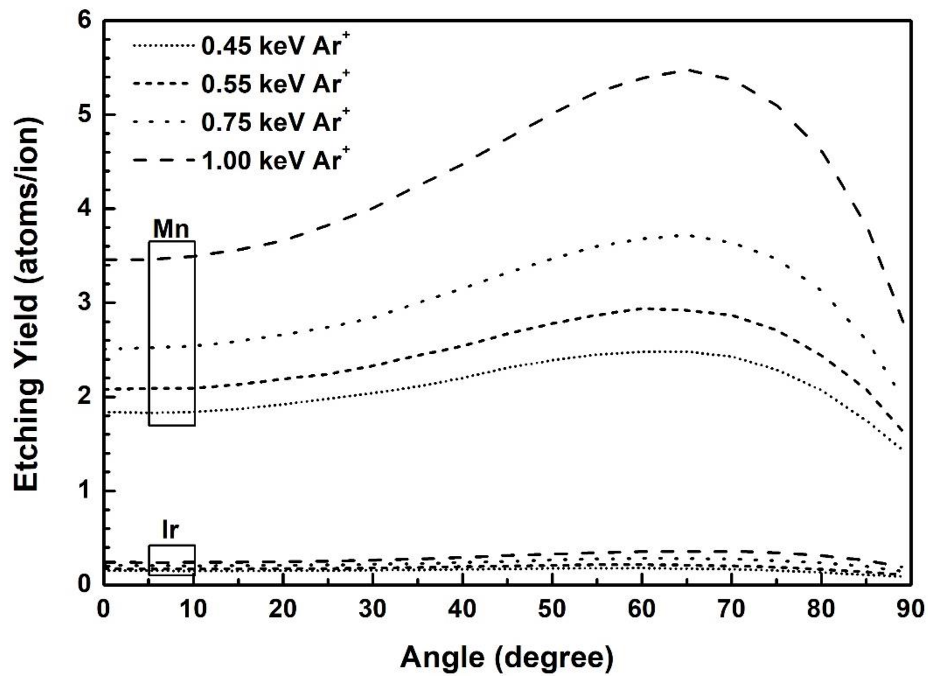

Figure 22 Plots of the calculated etching yields versus angle of the argon ions incident on $Ir_{21}Mn_{79}$ material using SRIM.

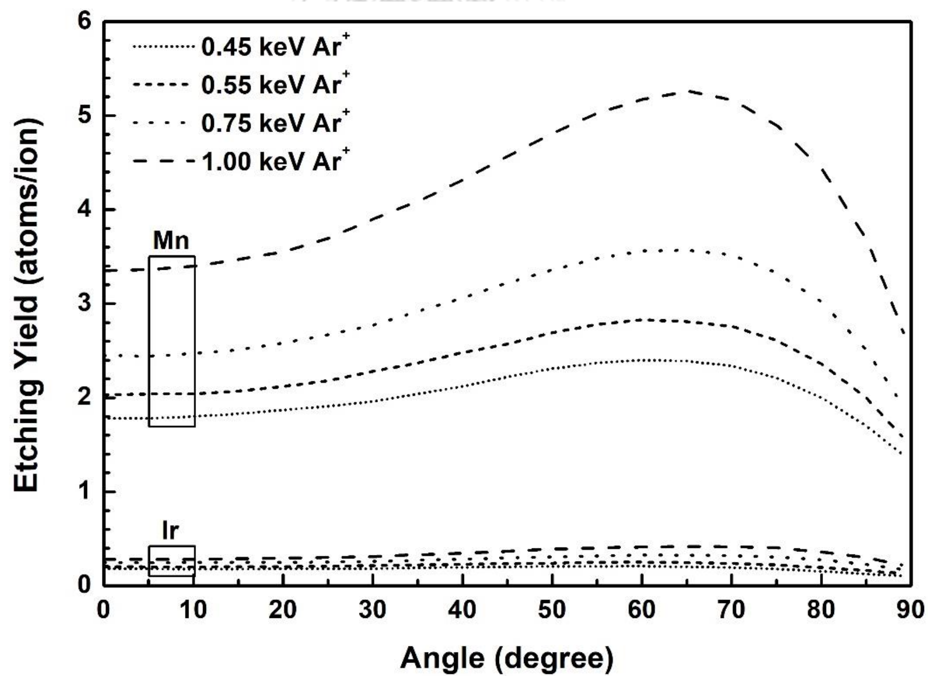

Figure 23 Plots of the calculated etching yields versus angle of the argon ions incident on $Ir_{24}Mn_{76}$ material using SRIM.

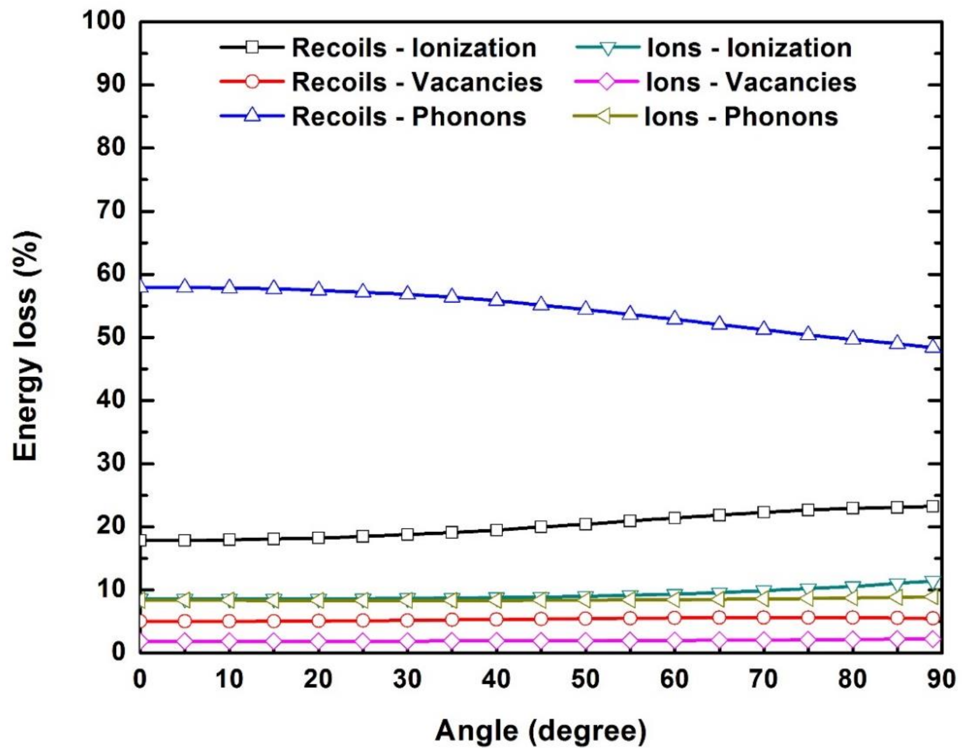

Figure 24 Plots of energy loss of incident ions.

Figure 24 showed the plots of the ion energy losses in $Co_{90}Fe_{10}$ material versus the ion incident angles from the calculations. The summation of the energy loss at any angle was normalized to 100%. At a normal angle of incident ions, ions can through into the surface of target plentifully. Those ions can make the recoil atoms release phonons at most. Thus, phonons which were occurred from recoil atoms was the most at this angle and decreased slightly as an incident angle increased. On the other hand, the ionizations from both ions and recoil atoms would be increased. The vacancies and phonons from ions constantly occurred which the vacancies from ions were the worst. The numbers of incident ions that penetrated into the surface of target were more than the ions that kicked the surface out. So the vacancies that were occurred from the incident ions directly were low.

Figure 25 Simulated etching yields of materials at +20°.- Figure **27** showed the etching yields of different materials in the reader/writer of HDD slider. The total etching yields (S_{Total}) of the homogeneous binary alloy materials were calculated by the following equation [28]:

$$S_{Total} = \frac{\alpha M_{\alpha} S_{\alpha} + \beta M_{\beta} S_{\beta}}{\alpha M_{\alpha} + \beta M_{\beta}} \quad (21)$$

where the α and β were the atomic percentage of target with their gram atomic mass of M_{α} and M_{β}, respectively.

These plots indicated that the total etching yields of the materials not only depended on the incident angle but also the ion energy and the classification of materials. For the ferromagnetic (CoFe and NiFe) and antiferromagnetic (IrMn) material, their yields were higher than the insulator (MgO). Since ions can penetrate deeper into the surface of the target at the incident angle of 90° to the surface, the yields were minimal with the lowest energy of ions. These yields would be applied with the experimental results to calculate the etching rates of all those materials.

จุฬาลงกรณ์มหาวิทยาลัย
CHULALONGKORN UNIVERSITY

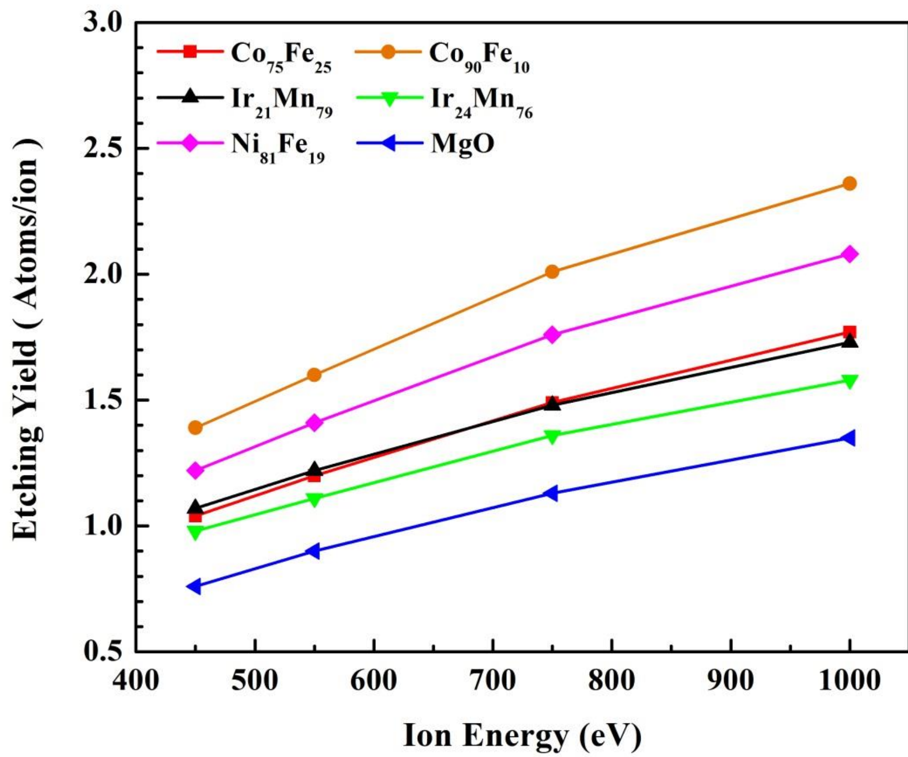

Figure 25 Simulated etching yields of materials at +20°.

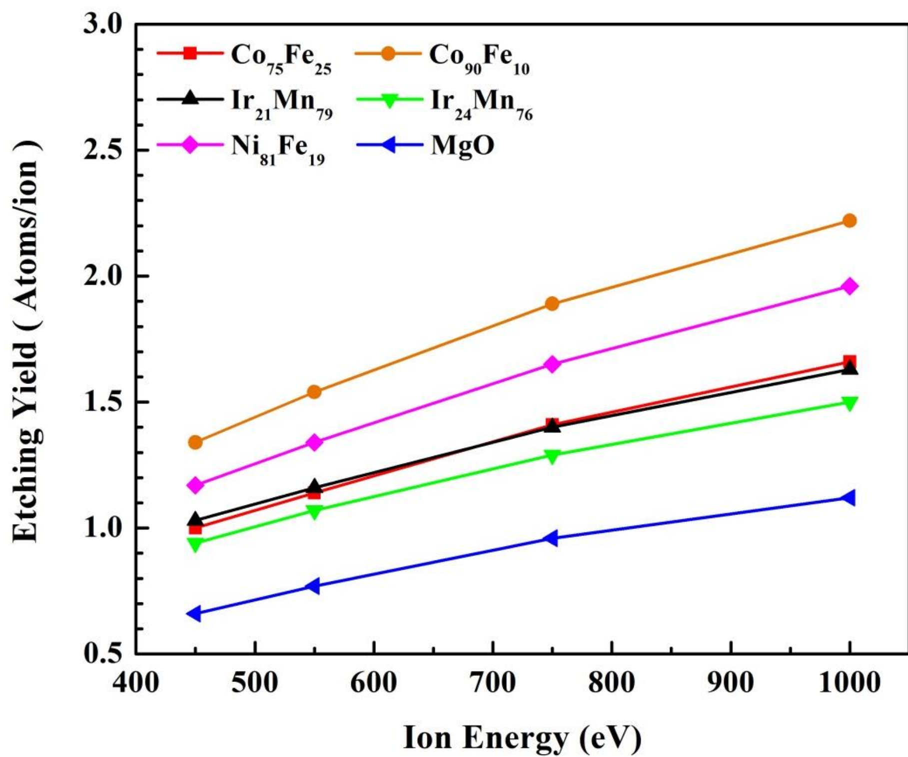

Figure 26 Simulated etching yields of materials at normal angle 0°.

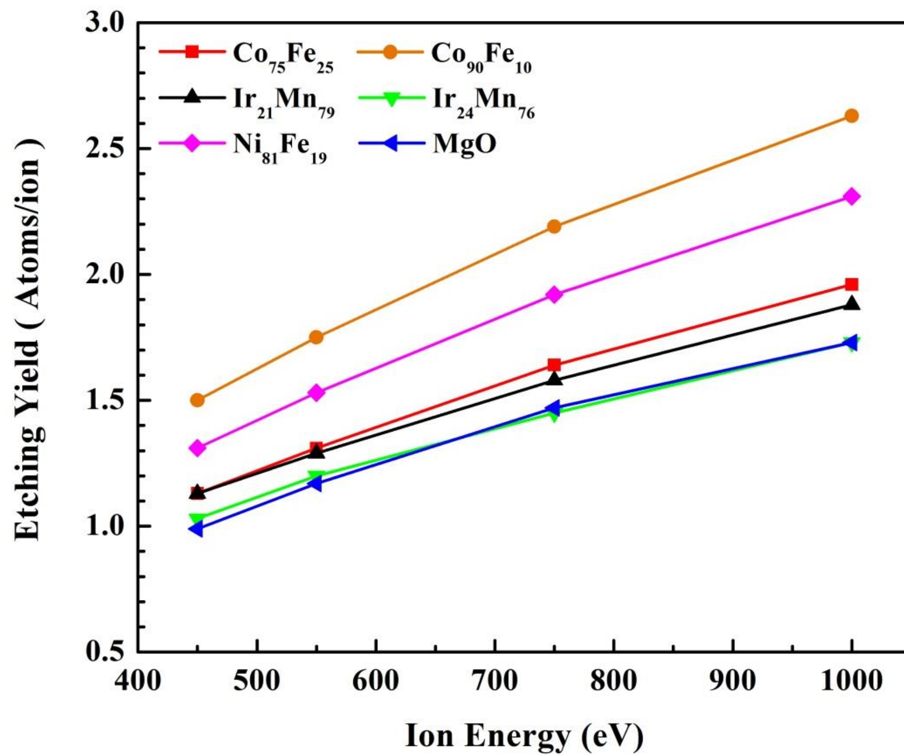

Figure 27 Simulated etching yields of materials at -30°.

จุฬาลงกรณ์มหาวิทยาลัย
CHULALONGKORN UNIVERSITY

4.2 Plasma characterizations in IBE system

The angular-dependent plasma I-V plotted at the impact angle of -20°, 0° (normal to the surface) and +30° were shown in Figure 28. The saturation part of those curves depended on an incident angle of ion beam. Floating potentials (V_f) of the plasma in this IBE system for all cases was calculate to be at about 3 V. As the ions from a source collided with the probe, the kinetic energy was transferred together with their charges and momentums. This created an ion current flow into the probe and probe circuit to be measured. Similar to electrons, they created an electron current into the probe circuit as positive bias was applied to the probe. At the normal angle to a surface, energetic ions can transfer their energy to a probe more than other angles. In case of the incident ion

was normal to the surface (0°), the maximum saturated ion current was at about 5 mA. This maximum saturated ion current also depended on the impact angle of the ions, as shown in Figure 28. The angle at +20° and -20°, it can be considered as the same angle. The difference of them was just the direction of an incident beam which ions came from the top or bottom of the normal vector to the surface. Note that, the value of saturated ion current at +20° was closer to the saturated ion current at normal angle than -30° position. The plasma potential (V_p) can be extracted from the I-V plot as shown in Figure 29. From the calculations, the plasma potential in this system was about 2.5 V. These parameters can explain the plasma behaviors in an industrial-size IBE system.

As seen from Figure 28, the I-V characteristic curve showed the effects from the ion/electron compensation by a PBN and electron filtered by the ion-optic grids in our IBE system. The obtained I-V characteristic curve was different from the ideal curve in the range of the measured electron currents. For this model of IBE system, a PBN was automatically operated during the measurement which made the I-V characteristic different from an ideal ion etching/sputtering system. The electrons were more released from PBN when the bias potential increased. This action caused an increasing of the electron current as the positive bias was applied to the plasma probe. Thus the electron currents did not saturate.

จุฬาลงกรณ์มหาวิทยาลัย
Chulalongkorn University

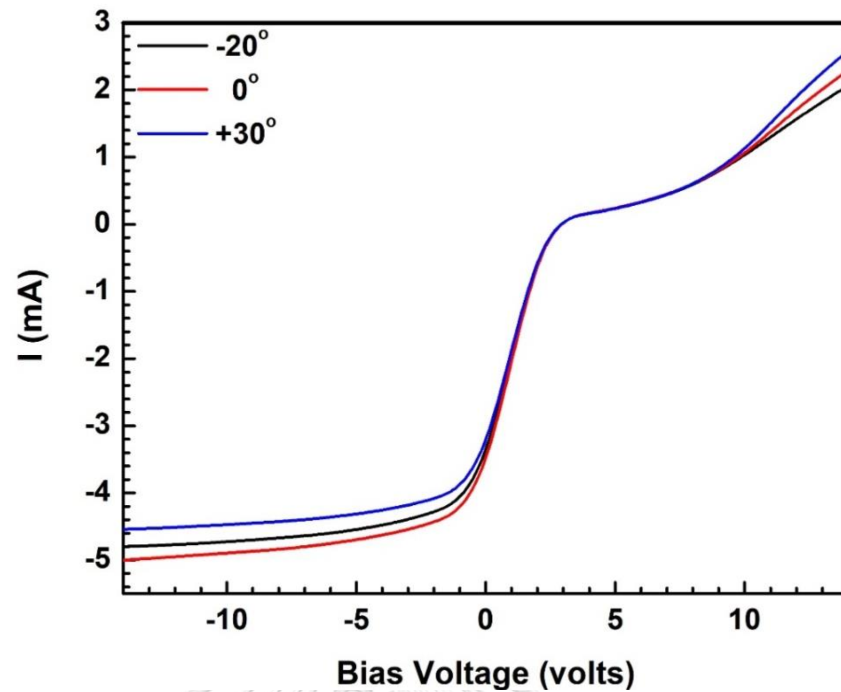

Figure 28 An I-V curve with a beam voltage, a beam current, an argon gas flow in PBN and an argon gas flow in a source are set as 400 volts, 800 mA, 6 sccm and 20 sccm respectively.

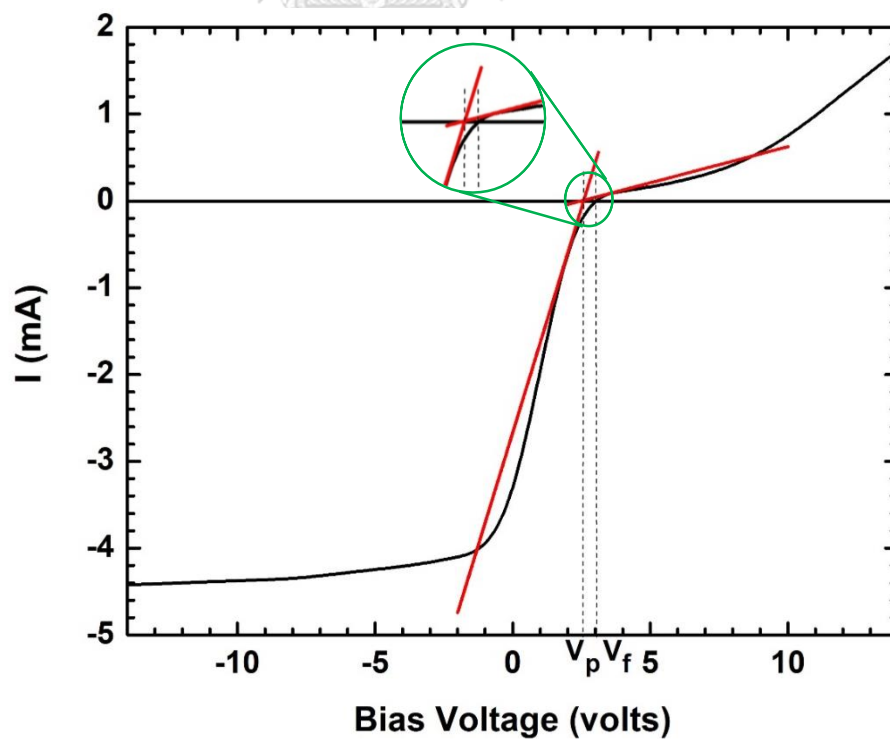

Figure 29 A floating potential and plasma potential observation.

4.2.1 Dependence on beam voltage and beam current

The potential difference between the first grid and a ground or “the beam voltage” can be estimated to the maximum kinetic energy of argon ions in the plasma. As the negative bias was applied to the plasma probe, the ions were attracted to move forward to the probe surface and be measured as ion current. However, the ions that had enough energy can only pass through the grids into an operating chamber. As the grid potential increased, the energy and the number of ions were not increased linearly. Thus, the energy and the number of ions did not only depend on the beam voltage, but also depend on other plasma factors such as beam current.

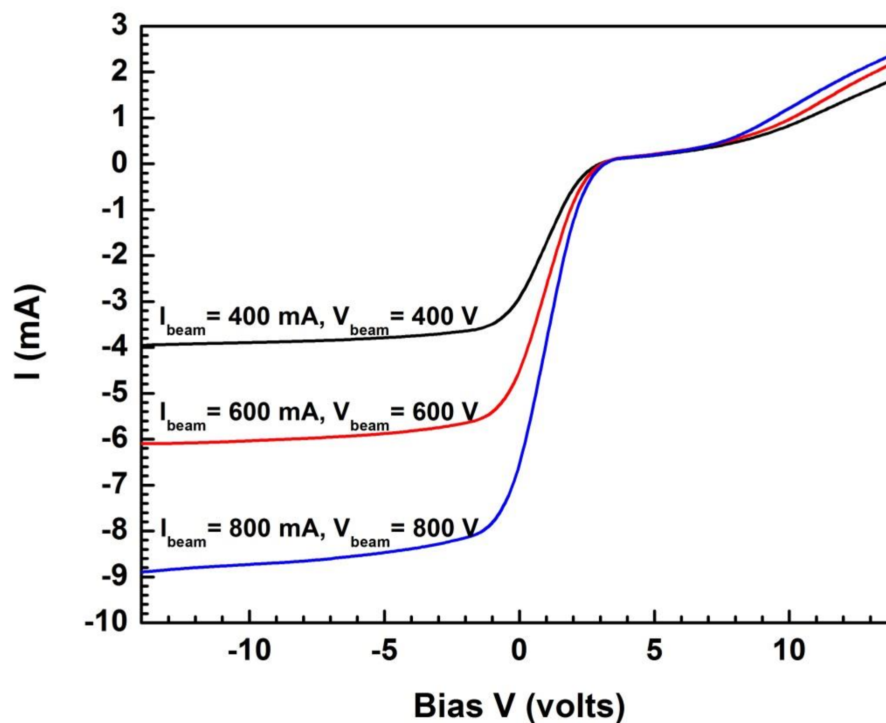

Figure 30 Plasma I-V curves of combinations of beam voltage and current, simultaneously with an argon gas flow in PBN and an argon gas flow in a source are set 6 sccm and 20 sccm respectively. The ion impact angle was at normal incident angle for all cases.

A comparison data between different setting of ion beam voltages and currents were shown in Figure 30. It clearly indicated that as the beam voltage and beam current were increased, the number of ions that can pass through the grids was obviously increased. The plasma flat probe can detect more ion current when these two factors increased.

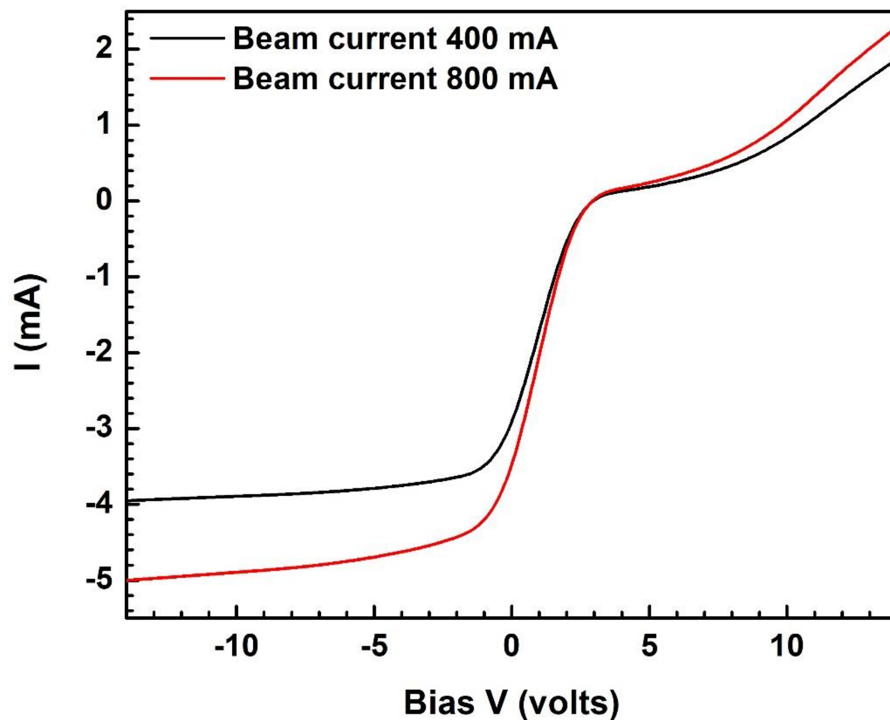

จุฬาลงกรณ์มหาวิทยาลัย
Chulalongkorn University

Figure 31 Plasma I-V curves at different beam currents with a beam voltage, an argon gas flow in PBN and an argon gas flow in a source are set as 400 V, 6 sccm and 20 sccm respectively. The ion impact angle was at normal incident angle for all cases.

Thus, the beam current was an important major parameter to set and tune the number of plasma species in an ion source. In order to generate the plasma at the ion source (ion gun), a high voltage current was biased to accelerate free electrons. Excited free electrons then ionized the argon gas molecules that were fed into an ion source and the plasma occurs, eventually. In our experiment, the beam current was increased from 400 mA to 800 mA with the fixed beam voltage of 400 V causing the amount of plasma

species started to rise up. This increased the number of energetic ions that though from grids to a chamber. As the beam current was increases, the total number of ions in the chamber that can be accelerated by the grids was also increased.

As seen in Figure 31, the saturated ion current was at about 4 mA with the beam current fixed to 400 mA and increased to about 5 mA as the beam current increased to 800 mA. This can cause an increasing in total etching rate of the system. Note that, even the saturated ion current was different, a floating potential and the saturated electron current of both cases were almost the same. Although the number of electrons that was generated from the ionization process in an ion source was much, it cannot pass a set of ion-optic grids into an operating chamber.

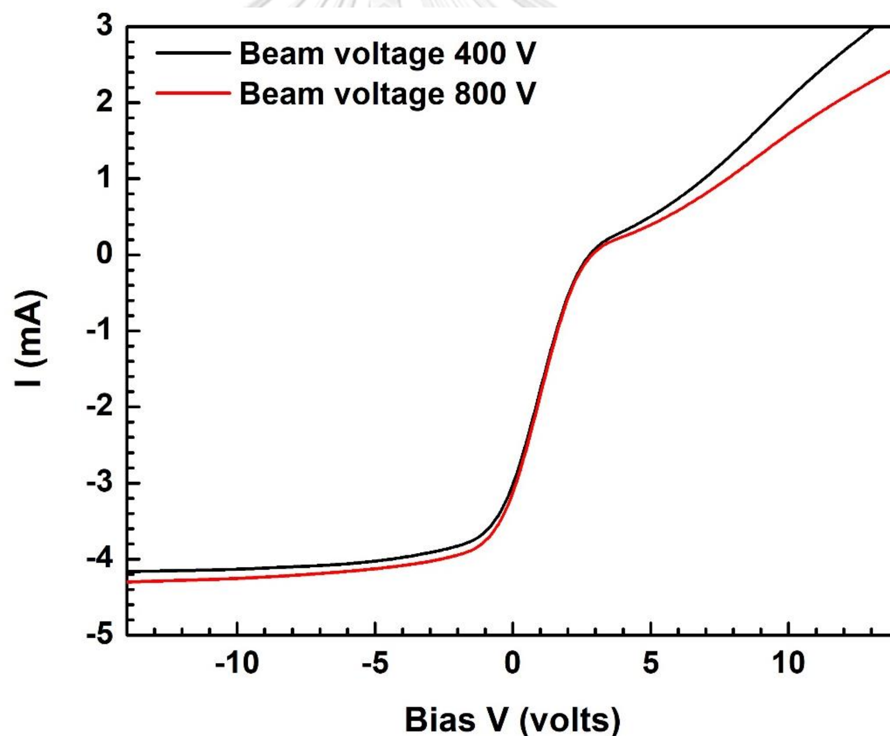

Figure 32 Plasma I-V curves at different beam voltages with a beam current, an argon gas flow in PBN and an argon gas flow in a source are set as 400 mA, 6 sccm and 20 sccm respectively. The ion impact angle was at normal incident angle for all cases.

To study the effect of the grid beam voltages, the plasma I-V curves at different beam voltages were measured with a fixed ion beam current at 400 mA. The number of ions generated in the plasma source was considered constant. As the beam voltages were set at 400 V and 800 V, the plasma I-V curves from both conditions were shown in Figure 32. The result indicated that the beam voltage did not result in any change of the ion current. Even the grid voltage was increased twice, from 400 V up to 800 V, the saturated ion currents of both cases were still remained almost the same. This can be due to the plasma current was fixed by the beam current via the grid potential. On the other hand, the saturated electron current was increased when a voltage biased to a screen grid was decreased. This phenomenon may be caused by a small electric field between the first two grids, confined electrons in an ion source of the system.

4.2.2 Dependence on PBN

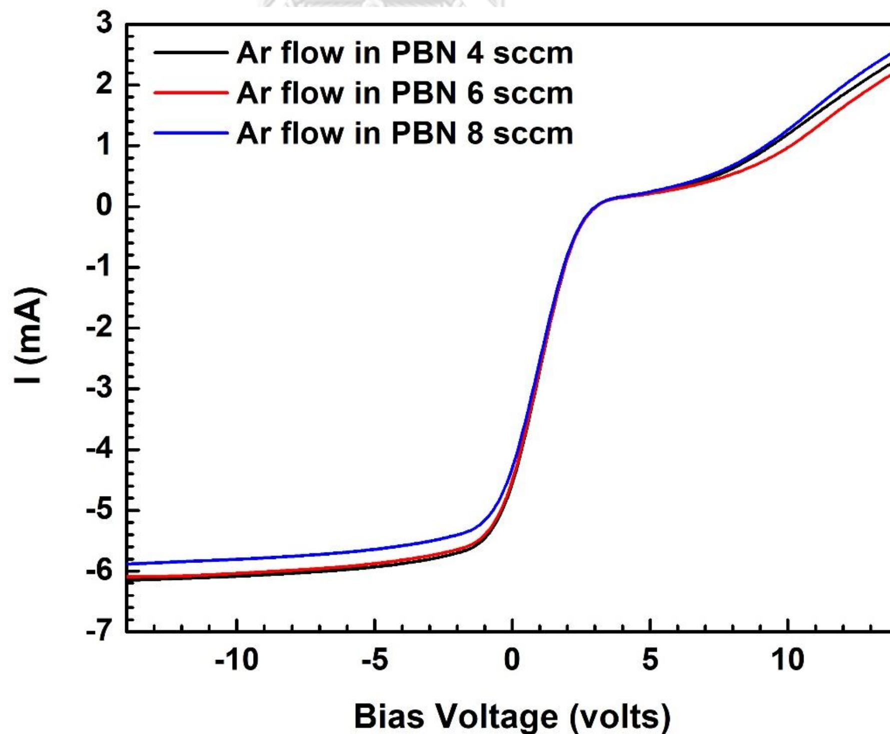

Figure 33 An I-V curve with a beam current, beam vlotage and an argon gas flow in a source are set as 600 mA, 600 V and 20 sccm respectively at normal incident angle.

For all of I-V curves, the floating potentials of each condition were about 3 volts. Ion saturations went on in the same way. They saturated at about -6 mA. In a range of electron saturation, a blue and black curve overlapped each other while the red curve – condition in the actual process – was less. If there was a small amount of electrons in a chamber, the electron current would less saturate than the system having a lot of electrons. In this system, the PBN would work automatically when there was some plasma in a chamber. The number of electrons that was released from a PBN increased slightly even if the number of plasma was much. Thus, there was no any difference in the electron saturation part as seen in Figure 33.

4.2.3 Dependence of an Argon flow in ion source

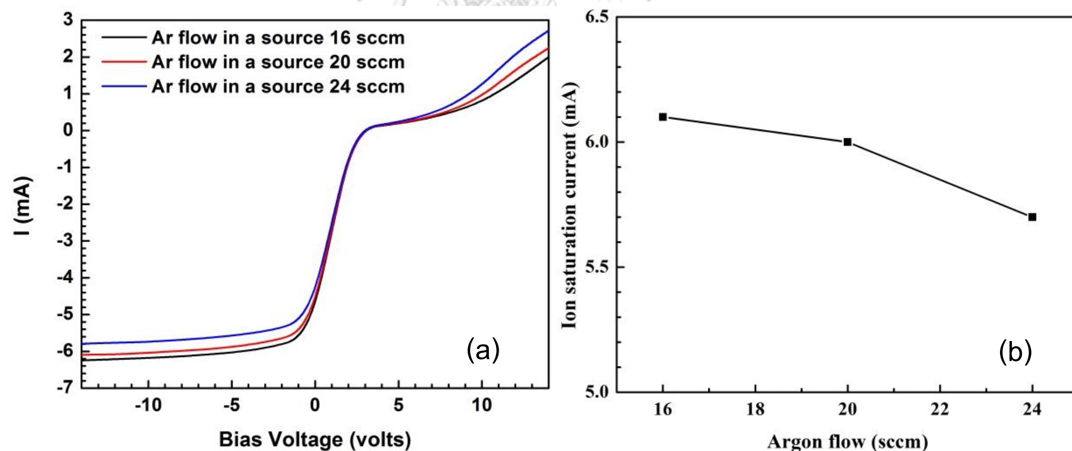

Figure 34 (a) An I-V curve with a beam current, beam voltage were set as 600 mA, 600 V and an argon gas flow in a source were 6 sccm respectively at normal incident angle. (b) Plots between I_{is} and argon flow in an ion source.

The argon gas that was fed into the ion source was ionized and generated the plasma. Theoretically, the increasing of the flow rate of argon affected the number of ions and electrons in the ion source. The ion currents into the circular flat probe were very

close as shown in the Figure 34(a). Although the argon was more fed into an ion source, the number of ion passing into the operating chamber depended on the beam current. In this case, the beam current was fixed. Thus the number of ion inside the chamber should constant. But our measured ion saturation currents increased a little bit as shown in Figure 34(b). It may be caused the increase of rate flows. When the argon was flowed fast, the ions were generated slightly. The ion saturation current at the rate flow of 24 sccm was lower than the ion saturation current at the rate of 16 sccm which were used in the real process. In the actual fabrication process, the difference of these ion saturation currents did not affect to the etching process. So the rate of argon flow was not affected to the number of ions in the chamber linearly. The ion saturation currents thus rarely were affected.

4.3 Ion current density calculations

The ion current density (j_p) was calculated for finding of etching rates of different materials in the TMR device structure in the following section. The simple definition of j_p is the rate of ion currents passing into a probe per area of a flat probe. During the plasma measurement, the ions were collected by the flat plasma probe with the surface area of 11.06 cm^2 (shown in Figure 35(a)). The summary of the ion saturation currents from experiments were reported in Table 3.

จุฬาลงกรณ์มหาวิทยาลัย
Chulalongkorn University

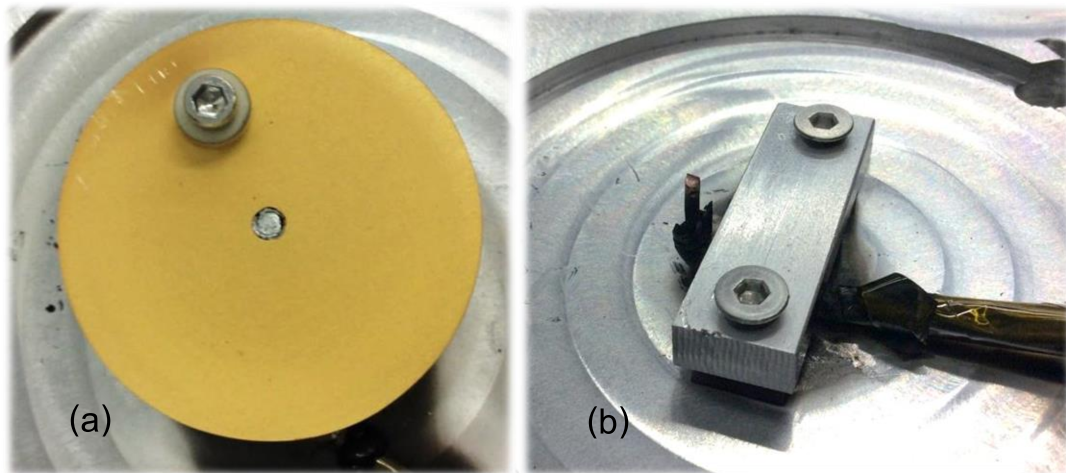

Figure 35 The (a) circular-flat probe and (b) wire probe used in measurements.

Table 3 The obtained ion saturation current from experiments with the argon flow in an ion source and PBN are 20 sccm and 16 sccm, respectively.

Condition	V_{beam} and I_{beam}	Ion saturation current (mA)		
		+20°	0° (Normal)	-30°
(1)	400 V, 400 mA	3.8	3.8	3.5
(2)	600 V, 600 mA	6.0	6.0	5.6
(3)	800 V, 800 mA	9	8.8	7.8
(4)	800 V, 400 mA	4.5	4.4	4.6
(5)	400 V, 800 mA	4.7	4.8	4.6

จุฬาลงกรณ์มหาวิทยาลัย
Chulalongkorn University

Table 4 The calculated ion current densities (j_p) with the argon flow in an ion source and PBN are 20 sccm and 16 sccm, respectively.

Condition	V_{beam} and I_{beam}	Ion current densities (mA/cm^2)		
		+20°	0° (Normal)	-30°
(1)	400 V, 400 mA	0.34	0.34	0.32
(2)	600 V, 600 mA	0.54	0.54	0.51
(3)	800 V, 800 mA	0.81	0.80	0.71
(4)	800 V, 400 mA	0.41	0.40	0.42
(5)	400 V, 800 mA	0.42	0.43	0.42

As the beam voltage and current were increased simultaneously, both the ion energies and numbers of ion were increased as well. From the conditions (1), (2) and (3) in

จุฬาลงกรณ์มหาวิทยาลัย
Chulalongkorn University

Table *4*, even though the ion current density values depended on both the beam voltage and current, the dependence of angle to these densities was disordered. Moreover, there was no any difference of ion current densities from a voltage-current alternation as shown in the conditions (4) and (5).

4.4 Etching rate calculations

The following etching rate of the target with molecular weight M [g/mol] and density ρ [g/cm^3] can be calculated by the expression;

$$\text{Sputtering / Etching rate} = 62.2 \frac{M}{\rho} S j_p$$

where S is a sputtering yield [atoms/ion] and

j_p is primary ion current density [mA/cm^2].

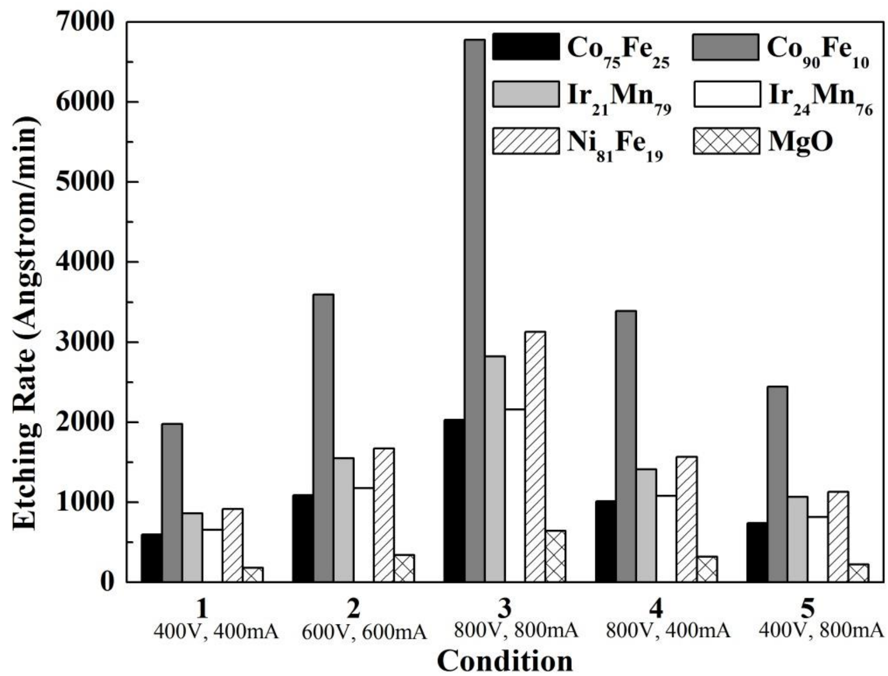

Figure 36 Etching rates of materials which are ordered by the conditions in the actual process. These rates are calculated by using the incident angle of +20º.

จุฬาลงกรณ์มหาวิทยาลัย
CHULALONGKORN UNIVERSITY

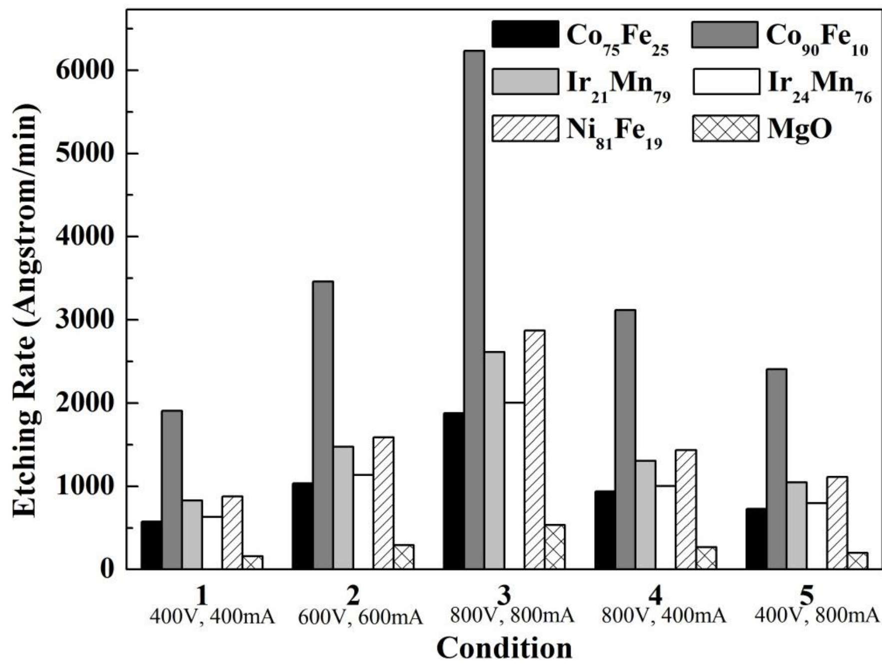

Figure 37 Etching rates of materials which are ordered by the conditions in the actual process. These rates are calculated by using the incident angle of 0º.

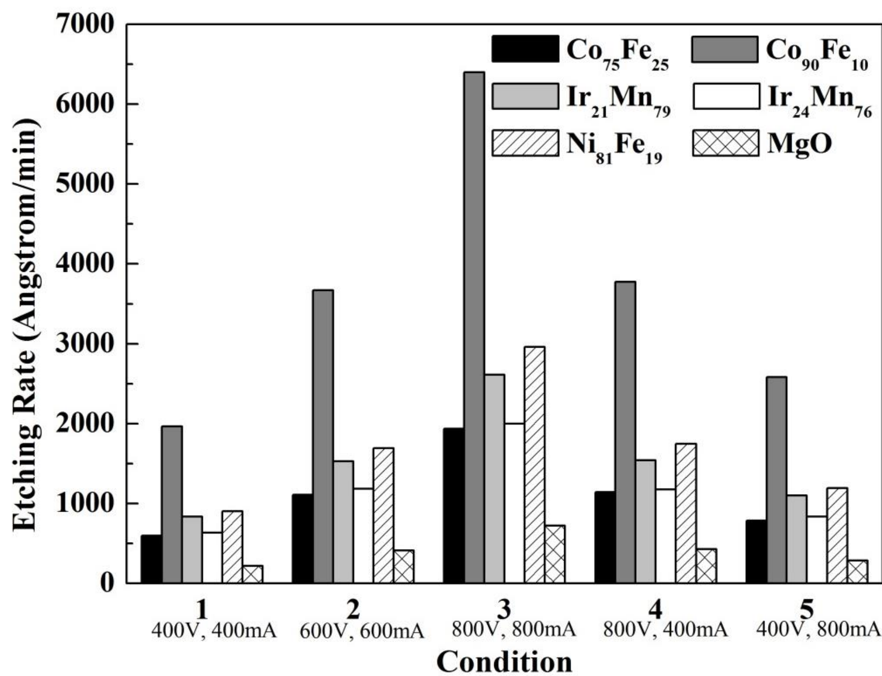

Figure 38 Etching rates of materials which are ordered by the conditions in the actual process. These rates are calculated by using the incident angle of -30º.

The details of each condition in Figure 36, 37 and 38 were shown in the Table 4. These conditions were used in our experiments, following the actual etching process of the HDD slider. For conditions (1), (2) and (3), the energy of ions were varied from the smallest to the biggest which were 400 V, 600 V and 800 V respectively. The changes of angle did not result in the change of ion current densities. Since the beam voltage represented the energy of ion beam, the etching rate of material depended on the increase of ion energy which has been used. The beam voltage in the conditions (3) and (4) was fixed at 800 V but their beam currents were very different. For the condition (4), although the beam voltage was much, the current that was used to generate the plasma was low. So the number of ions that can through from the source was limited. The detected etching rate in condition (4) thus was much less than in the condition (3). The effect of beam voltage to the etching rate was considered by the comparison of the conditions (3) and (5). The graphs showed clearly if the beam voltage increased, the etching rates rose as well.

The etching rates of different materials in TMR structure at different etching conditions were illustrated in Figure 36, 37 and 38. The results showed that the insulator or thermal barrier material such as MgO had a low etching rate compared to other materials. This can be due to the MgO is the ionic compound which Mg and O are bonded with the ionic bond. This bonding is a type of chemical bond that involves the electrostatic attraction between the oppositely charged ions. Otherwise, the other materials were the metal compound which can be easily etched by energetic ions.

The difference in the composition of the materials can also affect the total etching rate of the materials, as can be seen from the results of CoFe and IrMn materials in Figure 36, 37 and 38. This was due to because the opportunity in etching more occurs with the main atomic composition in compounds than others. As the much difference of the atomic ratio, it resulted in both the wide spaces and the far distance between same atoms. If the atoms were far each other, there was a soft interaction between them. Those atoms can be etched easily. Compare between the same type of materials, CoFe and NiFe, both were classified as magnetic materials. The different in etching rate of these 2 magnetic

materials were varied due to their compositions. In the condition (3) of Figure 36, the etching rates of $Co_{75}Fe_{25}$, $Ni_{81}Fe_{19}$ and $Co_{90}Fe_{10}$ were approximately 2000, 3100 and 6800 Å/min, respectively. The composition of $Co_{75}Fe_{25}$ and $Ni_{81}Fe_{19}$ were near. Their etching rates were closed which were less than the $Co_{90}Fe_{10}$'s.

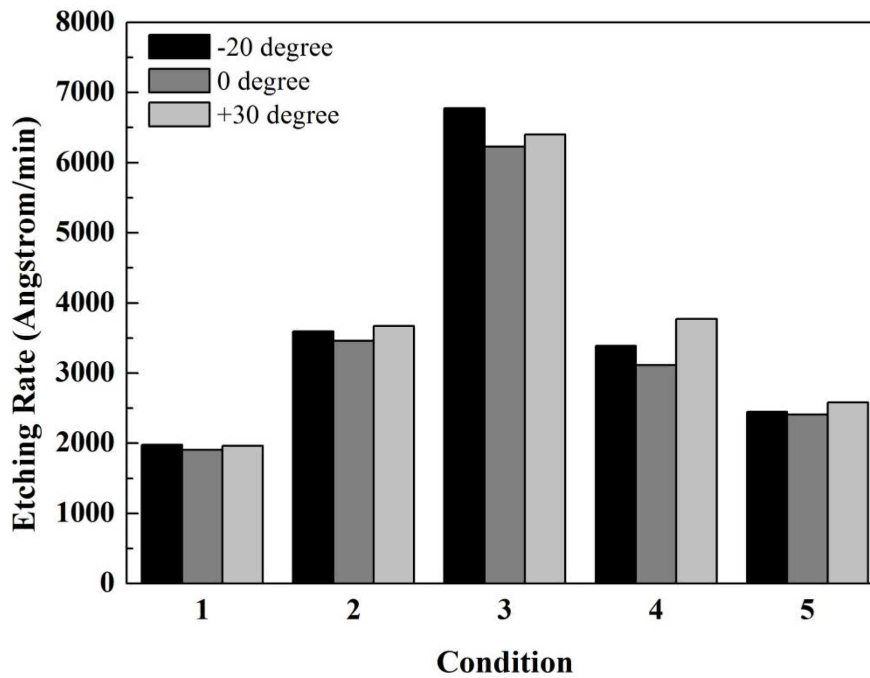

Figure 39 Etching rate of $Co_{90}Fe_{10}$ material.

จุฬาลงกรณ์มหาวิทยาลัย
CHULALONGKORN UNIVERSITY

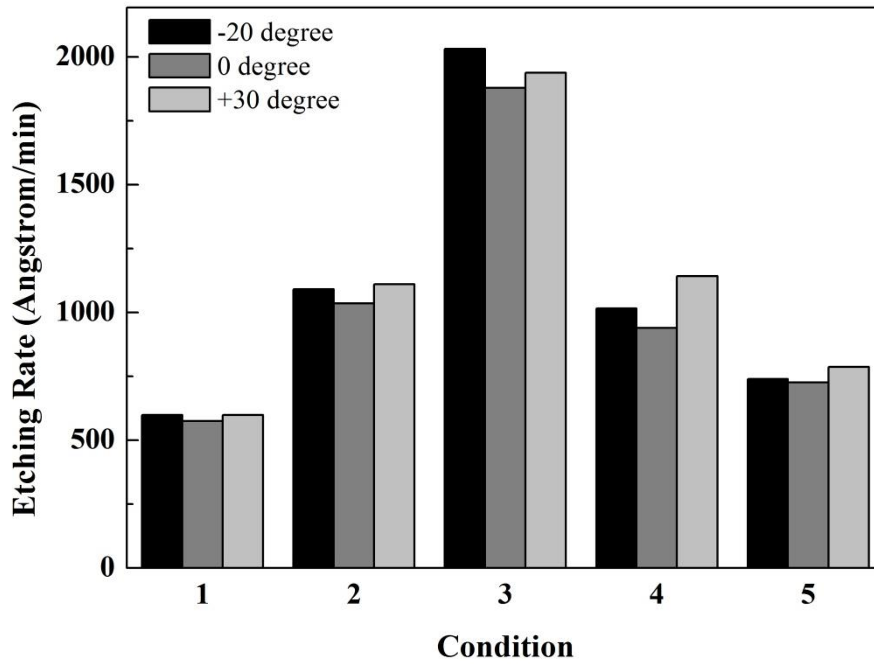

Figure 40 Etching rate of $Co_{75}Fe_{25}$ material.

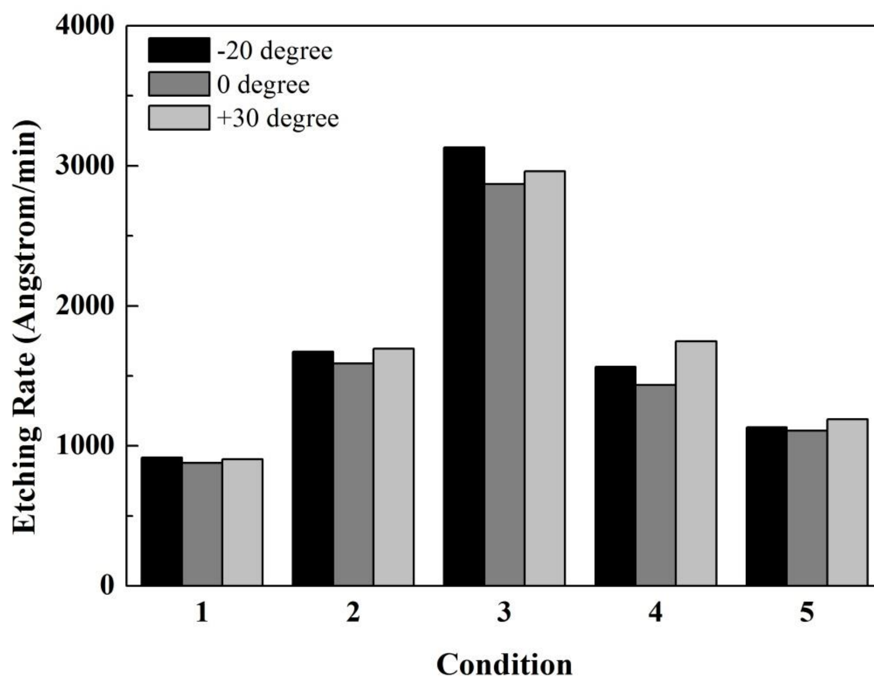

Figure 41 Etching rate of $Ni_{81}Fe_{19}$ material.

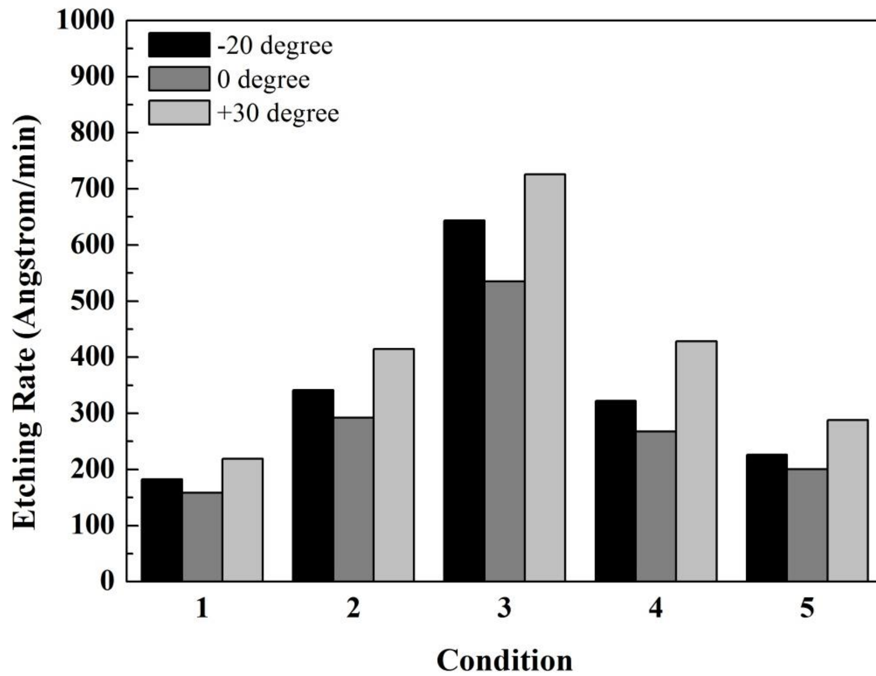

Figure 42 Etching rate of MgO material.

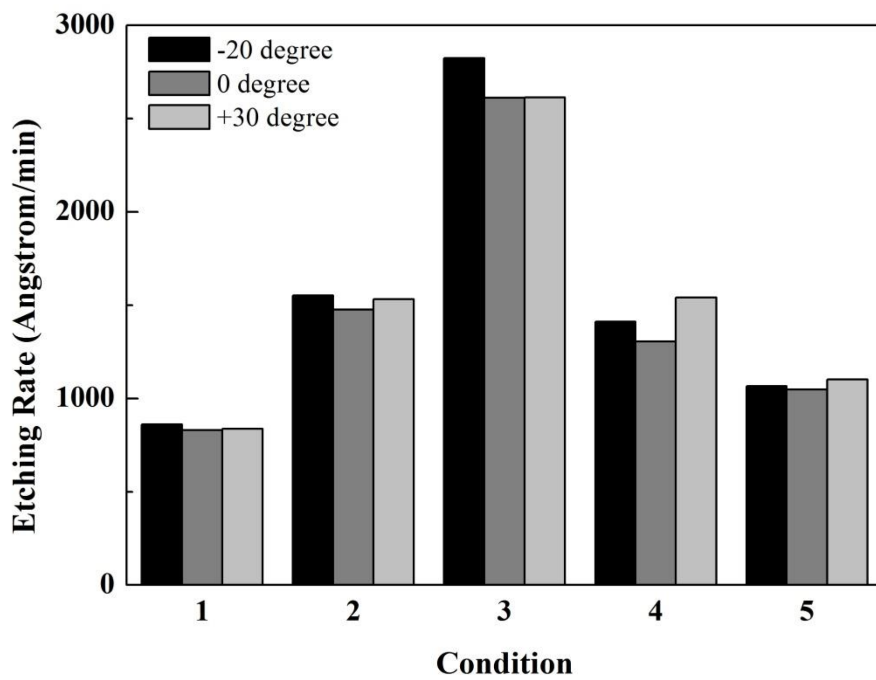

Figure 43 Etching rate of $Ir_{21}Mn_{79}$ material.

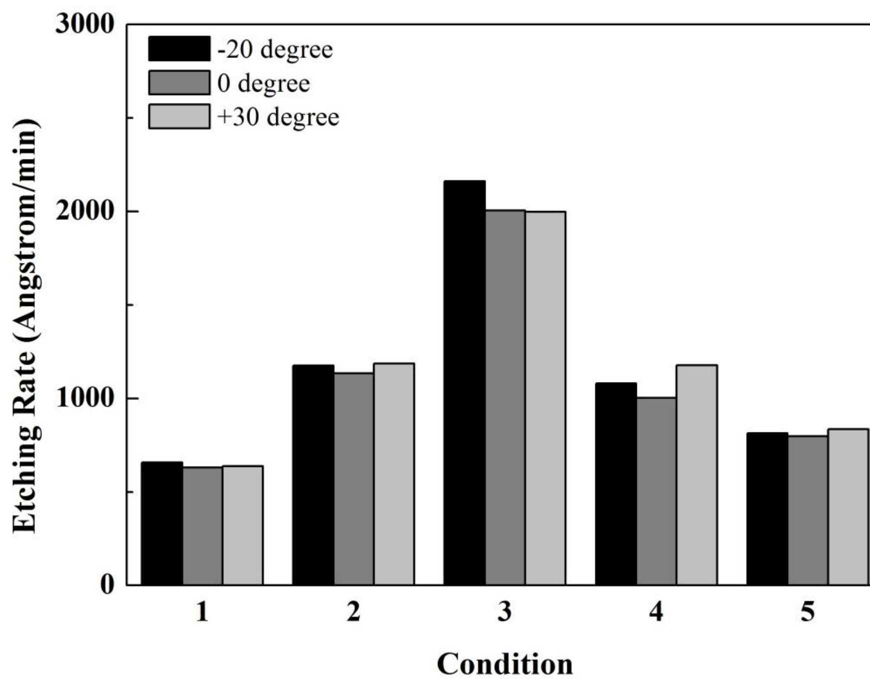

Figure 44 Etching rate of $Ir_{24}Fe_{76}$ material.

จุฬาลงกรณ์มหาวิทยาลัย
Chulalongkorn University

Figure 39 - 44 showed the dependence of incident angle of ion to the etching rate of different materials in TMR structure. The ions can penetrate deeper into the target as they come closer to the normal direction. The etching rates of the angle position at -30º and +20º were almost the same.

Most of calculated etching rate values were close to the etching rates in the actual process [6]. However, the difference between the calculated etching rates and actual etching rates may be due to the mechanism of the actual process. In the actual process, the sample holder was always rotated and tilted during the etching. The rates of etching can be measured as the average value for all of the samples. In this work, the probes were placed facing direct to the ion beam during the measurement without rotation. Another reason was that the electrical conductivity of the probe was much better than the actual sample which composed of many materials on AlTiC substrate. This issue can

make the measured etching rates slightly higher than actual values obtained from the electron microscopy results after etching.

จุฬาลงกรณ์มหาวิทยาลัย
Chulalongkorn University

CHAPTER V
SUMMARY AND CONCLUSION

In this thesis, the plasma characteristic and ion etching performance in the IBE system that used in HDD slider fabrication were studied. The etching yield, % energy loss and the number of backscattered ions of the reader and writer materials in TMR device structure were calculated by using the Monte Carlo-based simulation package, SRIM. Those materials were $Ir_{24}Mn_{76}$, $Ir_{21}Mn_{79}$, MgO, $Co_{90}Fe_{10}$, $Co_{75}Fe_{25}$ and $Ni_{81}Fe_{19}$. They were classified as ferromagnetic (CoFe and NiFe), antiferromagnetic (IrMn) and insulator (MgO). The calculated results showed that the maximum etching yields were optimized at the incident angle between 60° and 70°. The atomic ratio of elements which was the composition of binary alloy compounds affected to the values of the etching yield of them directly. If the atomic ratio of the elements was close to each other, the values of etching yields of each material were shifted toward each other. On the other hand, the yield would be much different if the ratio was not close to unity. The percentage of incident ions that transformed to backscattered ions was getting higher as the incident angle approaches 90°.

The plasma characterizations were done on the industrial-size IBE system to be able to get more information about the etching process. The plasma I-V characteristic curves obtained from the measurement were slightly different from the ideal curve that normally obtained from the sputtering process. This was due to the PBN that was installed in this IBE system. The function of this PBN was to balance the charge in a beam on the target surface. Thus, the saturation electron current could not be reached.

จุฬาลงกรณ์มหาวิทยาลัย
Chulalongkorn University

The increasing of etching yield depended on the ion energy and composition of the composite materials. Increasing the ion beam voltage and current caused more energetic ions travel plentifully through grids from an ion source which increased more accelerated ions toward the surface of the target. The ion current densities of each material were calculated mathematically. The changes of parameters, such as the beam voltage, beam current, incident angle argon flow in a PBN and in a source had different effects to the IBE processes. The argon flow rate that fed into a PBN and a source to generate the plasma could increase the number of ions from the ionizations. The beam voltage did not result in any changes of the ion current but increased the kinetic energy of ions that were accelerated toward the target. The percentage of incident ions that were transformed to backscattered ions was getting higher as the incident angle approaches 90°. The energy and the number of ions which were through the grids depended on the plasma beam current.

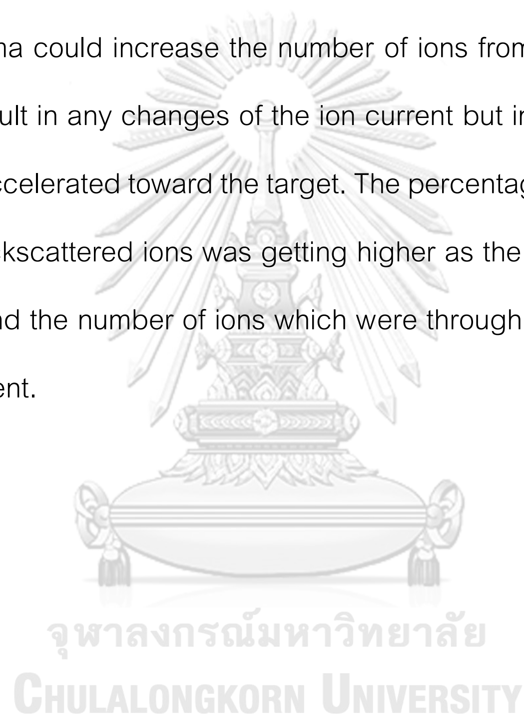
จุฬาลงกรณ์มหาวิทยาลัย
Chulalongkorn University

REFERENCES

1. Zhu, J.-G.J., *New heights for hard disk drives.* Materialstoda, Elsevier 2003: p. 22-30.
2. Parkin, S., et al., *Exchange-Biased Magnetic Tunnel Junctions and Application to Nonvolatile Magnetic Random Access Memory (Invited)*. Vol. 85. 1999. 5828-5833.
3. Zhu, J.-G. and C. Park, *Magnetic tunnel junctions.* Materials Today, 2006. 9(11): p. 36-45.
4. Bo Liu, M.Z., Shengkai Yu, Leonard Gonzaga, Hor Y. Sim, *Femto slider: Fabrication and Evaluation.* IEEE, 2002.
5. Ching F. Yong, E.Y.K.N., Wei D. Zhou, and Wan K. Ng, *Design and Modeling of Femto Air Bearing Slider*. Scientific Research, 2010: p. 841-854.
6. Nobuto Fukushima, T.S., Toshiaki Wada, Yasuhiro Horiike, *New reactive ion etching process for HDD slider fabrication.* IEEE Transactions on Magnetics, 1996. 32: p. 3786-3788.
7. S. Ikeda, J.H., Y. Ashizawa, Y. M. Lee, K. Miura, H. Hasegawa, M, Tsunoda, F. Matsukura, H. Ohno, *Tunnel magnetoresistance of 604% at 300 K by suppression of Ta diffusion in CoFe/MgO/CoFeB pseudo-spin-valves annealed at high temperature*. Applied Physics Letters, 2008. 93.
8. J. R. Childress, M.J.C., S. I. Kiselev, J. A. Katine, S. Maat, N. Smith, *Dual current-perpendicular-to-plane giant magnetic recording heads with reduced sensitivity to spin-torque-induced noise.* Journal of Applied Physics, 2006. 99.
9. Toyoo Miyajima, R.I., Koichiro Honda, Mineharu Tsukada, *Evaluation of devices and materials by transmission electron microscopy.* FUJITSU Science Technology Journal, 2010. 46: p. 273-279.
10. John P. Greene, J.N., George E. Thomas, Stacey L. Schiel, *Noble gas sputterinf calculations using TRIM.* Nuclear Instruments and Methods in Physics Research A, 1997: p. 91-98.

11. Canada, D.R.E.S. *Data Recovery Process from hard disk drive (HDD) [Online]* 2017; Available from: http://www.datarecoveryexpert.ca/Hard_drive_recovery.html.

12. Mee, C. and E.D. Daniel, *Magnetic Recording Technology*. 1996: McGraw-Hill Companies,Incorporated.

13. Kubina, J. *Hard disk drive performance characteristics [Online]*. 2006 23 August 2006; Available from: http://www.wikiwand.com/en/Hard_disk_drive_performance_characteristics.

14. Damjanović, Ž. *HDD head assembly [Online]*. Available from: http://hddsurgery.com/blog/hdd-head-assembly.

15. Goldston, R.J. and P.H. Rutherford, *Introduction to Plasma Physics*. 1995: CRC Press.

16. Chen, F.F., *Introduction to Plasma Physics*. 2012: Springer US.

17. Tungasmita, S., *Growth of wide-band gap AlN and* $(SiC)_x(AlN)_{1-x}$ *thin films by reactive magnetron sputter deposition*, in *Department of Physics and Measurement Technology*. 2001, Linköpings universitet.

18. McNeil, J.R., J.J. McNally, and P.D. Reader, *11 - Ion Beam Deposition A2 - Seshan, Krisna*, in *Handbook of Thin Film Deposition Processes and Techniques (Second Edition)*. 2001, William Andrew Publishing: Norwich, NY. p. 463-499.

19. Harper, J.M.E., *6 - Ion Beam Etching A2 - Manos, Dennis M*, in *Plasma Etching*, D.L. Flamm, Editor. 1989, Academic Press: Boston. p. 391-423.

20. Jaeger, R.C., *Introduction to Microelectronic Fabrication*. 1988: Addison-Wesley Publishing Company.

21. Carlström, C.-F., *Ion Beam etching of InP based materials*, in *department of Microelectronics and Information Technology*. 2001, Royal Institute of Technology.

22. Vawter, G.A., *Ion Beam Etching of Compound Semiconductors*, in *Handbook of Advanced Plasma Processing Techniques*, R.J. Shul and S.J. Pearton, Editors. 2000, Springer Berlin Heidelberg: Berlin, Heidelberg. p. 507-547.

23. Lejeune, C., J.P. Grandchamp, and O. Kessi, *Electrostatic reflex plasma source as a plasma bridge neutralizer.* Vacuum, 1986. 36(11): p. 857-860.

24. Chung, K.F., *Hydrogen sulfide as a potential biomarker of asthma.* Expert Review of Respiratory Medicine, 2014. 8(1): p. 5-13.

25. York, T.M. and H.-B. Tang, *Chapter 5 - Plasma Parameters and Regimes of Interaction*, in *Introduction to Plasmas and Plasma Dynamics*. 2015, Academic Press: Oxford. p. 87-98.

26. Merlino, R.L., *Understanding Langmuir probe current-voltage characteristics.* American Journal of Physics, 2007. 75: p. 1078-1085.

27. Ziegler, J.F., J.P. Biersack, and M.D. Ziegler, *SRIM, the Stopping and Range of Ions in Matter*. 2008: SRIM Company.

28. Pierson, K.W., et al., *Total sputtering yield of Ag/Cu alloys for low energy argon ions.* Nuclear Instruments and Methods in Physics Research Section B: Beam Interactions with Materials and Atoms, 1996. 108(3): p. 290-299.

จุฬาลงกรณ์มหาวิทยาลัย
Chulalongkorn University

APPENDICES

จุฬาลงกรณ์มหาวิทยาลัย
CHULALONGKORN UNIVERSITY

Appendix A

Conference Presentation

Napakan Wongpanit, P. O. Å. Persson and Sukkaneste Tungasmita. Etching behaviors of tunneling magnetoresistive (TMR) materials by ion beam etching system. *The 3rd International Conference on Applied Physics and Material Applications (ICAPMA2017)*, Pattaya, Chonburi, Thailand 31 May – 2 June, 2017 **(Poster presentation).**

จุฬาลงกรณ์มหาวิทยาลัย
CHULALONGKORN UNIVERSITY

VITA

Mr. Napakan Wongpanit was born on the 19th November 1991 in Chaiyaphum, Thailand. He finished high school from Mahasarakham University Demonstration School, Mahasarakham, then graduated his Bachelor's degree in Science-Physics major from Khonkaen University, Khonkaen in 2013, and continued his master's degree in Physics at Chulalongkorn University.